

國立交通大學

電信工程學系

碩士論文

在時變衰減通道下之結合通道估測與信號偵測
演算法和低密度同位元檢查碼解碼之遞迴系
統的編碼設計

LDPC Code Design for Joint Channel Estimation,
Symbol Detection and LDPC Decoding in
Time-Varing Fading Channels

研究生：賴沛霓

指導教授：伍紹勳

中華民國九十九年五月

在時變衰減通道下之結合通道估測與信號偵測演算法和低密度同位元
檢查碼解碼之遞迴系統的編碼設計

LDPC Code Design for Joint Channel Estimation, Symbol Detection and LDPC
Decoding in Time-Varying Fading Channels

研究生：賴沛霓

Student : Pei-Ni Lai

指導教授：伍紹勳

Advisor : Sau-Hsuan Wu

國立交通大學

電信工程學系

碩士論文

A Thesis

Submitted to Department of Communication Engineering

College of Electrical and Computer Engineering

National Chiao Tung University

in partial Fulfillment of the Requirements

for the Degree of

Master

in

Communication Engineering

May 2010

Hsinchu, Taiwan, Republic of China

中華民國九十九年五月

在時變衰減通道下之結合通道估測與信號偵測演算法 和低密度同位元檢查碼解碼之遞迴系統的編碼設計

研究生：賴沛霓

指導教授：伍紹勳

國立交通大學電信工程學系碩士班

摘要

在雷利衰減通道下，此研究利用結合通道估測與信號偵測演算法和低密度同位元檢查碼解碼之遞迴系統來幫助我們在沒有任何領航信號和訓練信號的情況下作解碼。然而在衰減通道下，低密度同位元檢查碼之變數節點間的相互關係會依據其通道衰減速度緩慢遞減。為了達成低密度同位元檢查碼的無迴圈條件，其變數節點間的獨立假設是必須的。因此在本研究中，所有連接至相同檢查節點的變數節點必須限制在不同的同調區間來達成上述獨立假設。而有限長度的低密度同位元檢查碼其效能會受到其所經歷的同調區間個數和衰減速度的影響。

LDPC Code Design for Joint Channel Estimation, Symbol Detection and LDPC Decoding in Time-Varying Fading Channels

Student: Pei-Ni Lai

Advisor: Sau-Hsuan Wu

Department of Communication Engineering
National Chiao Tung University

Abstract

Without using any pilot and training symbols, a serially concatenated turbo transceiver is proposed for joint channel estimation, symbol detection and LDPC decoding in Rayleigh fading channels. In fading channels, the dependence of variable nodes in the factor graph lingers slightly according to the fading speeds. However the independence assumption is necessary for the cycle-free condition of LDPC codes. Hence we added the design criterion that the variable nodes connected to the same check node are restricted to be in different coherence intervals to meet the constraint. The performance of finite-length LDPC codes would be affected both by the number of coherence intervals and the fading speed.

誌 謝

能夠順利完成論文，首先要感謝的是我的指導教授伍紹勳老師，在老師兩年多來耐心與細心的指導下，學習如何逐步完成研究，在研究過程中學習發現問題和思考問題，使我獲益良多。另外感謝實驗室所有的夥伴們，給予我研究上和生活上許多幫助。其中JK、Sazabi、Tina、Sony、Jason協助我許多關於研究上的問題，此外也感謝我的好朋友們宇君、筱雯、純平給予我許多精神上的支持和鼓勵，最後感謝默默支持我的家人們，因為他們的付出，讓我能夠心無旁騖且無後顧之憂的完成論文並取得碩士學位。



Contents

摘要	i
Abstract	ii
誌謝	iii
Contents	iv
List of Figures	vi
1 Introduction	1
2 System Model	3
2.1 System model : Transmitter structure	3
2.2 System model : Receiver structure	3
3 Joint Channel Estimation and Symbol Detection based on EM Algorithm	5
3.1 EM-based joint channel estimation and symbol detection in flat fading channels	5
4 RA Decoder	13
4.1 Design Criteria of LDPC Code	14
5 Combined EM-JED algorithm and LDPC Decoding	18
5.1 LDPC Decoding	18
5.1.1 Variable Nodes Analysis	19
5.1.2 Check Nodes Analysis	20
5.2 Combined EM-JED algorithm and RA decoder with LDPC Decoding	20

6	Density Evolution	23
7	EXIT Chart Analysis	31
8	Simulation Results	34
8.1	Performance of EM-JED algorithm in different fading speeds	34
8.2	Performance of combined EM-JED algorithm and LDPC decoding in fading channels	37
8.2.1	The performance of the same codeword length 12000 in different fading speeds	37
8.2.2	The performance of the same number of coherence intervals in different fading speeds	38
8.2.3	The performance of the same codeword length 120000 in different fading speeds	39
8.3	Performance of different degree profiles with density evolution analysis	40
9	Conclusions	46
	Bibliography	47



List of Figures

2.1	Transmitter Structure.	4
2.2	Turbo-like iterative receiver structure.	4
3.1	Illustration of JED algorithm.	12
4.1	The phase ambiguities associated with the channel estimates obtained with the EM-JED algorithm.	14
4.2	The RA encoder associated with the Tanner graph.	15
4.3	The Tanner graph of both LDPC encoder and RA encoder.	15
4.4	The performance of the regular (3,6) degree profile and codeword length 12000 in ideal fading channel.	17
5.1	Tanner graph of LDPC code.	19
5.2	The computation of extrinsic message q_{ij} at the variable node c_i	20
5.3	The computation of extrinsic message r_{ji} at the check node f_j	21
5.4	Illustration of the iterative procedure in the receiver.	22
6.1	Illustration of density evolution of the iterative receiver.	24
6.2	Illustration of half-iteration message passing at variable node in density evolution.	26
6.3	Illustration of half-iteration message passing at check node in density evolution.	27

6.4	The histogram of output LLRs passed from check nodes to variable nodes with regular (3,6) degree profile.	30
6.5	The histogram of output LLRs passed from check nodes to variable nodes with variable-irregular and check-regular degree profile.	30
7.1	Illustration of density evolution of the iterative receiver.	32
8.1	Performance of EM-JED algorithm in the fading speed 0.01.	35
8.2	Performance of EM-JED algorithm in the fading speed 0.005.	35
8.3	Performance of EM-JED algorithm in the fading speed 0.001.	36
8.4	Performance of EM-JED algorithm in different fading speeds.	36
8.5	Performance of the same codeword length 12000 in different fading speeds.	37
8.6	Performance of the same number of coherence intervals in different fading speeds.	38
8.7	Performance of the same codeword length 120000 in different fading speeds.	39
8.8	Performance of given regular-check degree profile which contains the minimum variable degree 2.	40
8.9	Performance of regular (3,6) LDPC code.	42
8.10	Performance of regular (4,8) LDPC code.	42
8.11	Performance of given regular-check degree profile with maximum variable degree 4.	43
8.12	Performance of given regular-check degree profile with maximum variable degree 7.	43
8.13	Performance of given regular-check degree profile with maximum variable degree 11.	44
8.14	Performance of given regular-check degree profile with maximum variable degree 19.	44
8.15	Performance of the overall generated regular-check degree profiles.	45

Chapter 1

Introduction

In wireless communications, data sequences are transmitted over time-varying fading channels. And the channel state information (CSI) is usually unknown at the receiver. Hence the channel estimation becomes an important task at the receiver. For easy channel estimation, the pilot and training symbols are often used. However, in fast fading channels, large number of training and pilot symbols would make the performance relative to the channel capacity degrades substantially. Pilot-symbol-aided or training sequence based channel estimation can be substituted by the blind channel estimation. The JED algorithm is firstly proposed in [1]. Based on the iterative procedure of EM algorithm [2], the JED algorithm is used to do joint channel estimation and symbol detection iteratively. Nevertheless, there are phase ambiguities associated with the channel estimates obtained with the EM algorithm of joint channel estimation and symbol detection. And the differential code is used here to solve this problem. Besides, the differential code can also serve as the inner code of a serially concatenated code in our system.

The low density parity check (LDPC) codes were firstly proposed by Gallager [3] in 1960. LDPC code is a linear block code which provides near-capacity performance. In 1981, the Tanner graph [4] is proposed as a bipartite graph to specify the calculation in error correcting codes. However the LDPC code is scarcely used until the mid-1990's.

The study of LDPC codes is rediscovered for its capacity-approaching performance [5–7]. In LDPC decoding [8], the message-passing algorithm (MPA), known as the sum-product algorithm (SPA), is used.

In [9, 10], the differential code is used with the LDPC code over flat Rayleigh fading channels and the channel estimation is not required in their system. In [11–13], the pilot symbols are employed in channel estimation over block fading channels. Combined EM-JED algorithm and LDPC decoding are performed iteratively without any pilot and training symbols in our system.

The density evolution [14] and EXIT chart [15] are often used to do the performance analysis of iteratively-decoded error-correcting codes, such as LDPC codes. These two methods are used to predict the performance of LDPC codes of the given degree profile without a numerical simulation. In [16–19], the convergence behavior of EXIT chart is explained. In [11], the EXIT chart analysis is used. The density evolution is modified with the *discretized density evolution* in [20]. In [12, 13], the density evolution is used to analyze the performance. The density evolution with Gaussian approximation [21] is employed in our performance analysis. The EXIT chart analysis of combined JED algorithm and LDPC decoding is referred to [16].

Chapter 2

System Model

2.1 System model : Transmitter structure

The transmitter structure is shown in Fig. 2.1. The information bits are firstly encoded by LDPC code. The output coded bits are then sent into DBPSK modulator. Here the differential modulator, also known as the RA code, serves as the inner code, and the LDPC code serves as the outer code of a serially concatenated turbo-like code. One thing to be noted is that there is no interleaver added between the LDPC encoder and DBPSK modulator. To prevent the short cycles from occurring in LDPC code and differential encoder, it would become much easier to satisfy our design criteria of the LDPC code by taking off the interleaver. The details are shown in Chapter 4.1.

2.2 System model : Receiver structure

A non-coherent time-varying fading channel is used in this paper. The received signal is given by

$$y_m = h_m x_m + n_m,$$

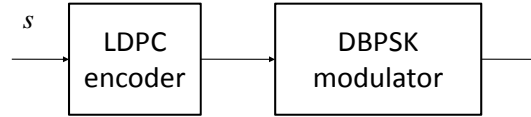


Figure 2.1: Transmitter Structure.

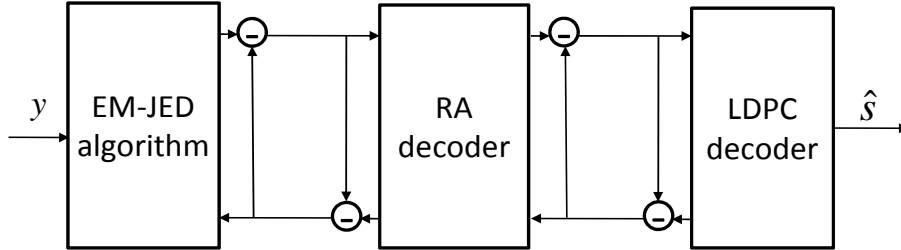
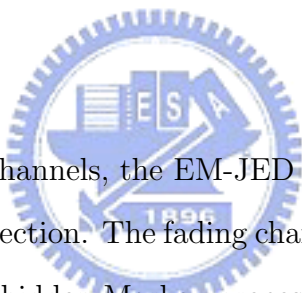


Figure 2.2: Turbo-like iterative receiver structure.

where x_m is the m th transmitted symbol, y_m is the received signal, h_m is the fading channel coefficient, and n_m is zero-mean and unit-variance complex Gaussian variables. A serially concatenated iterative receiver is shown in Fig. 2.2. The extrinsic message is iteratively passed between each block. All the extrinsic message is represented in log likelihood ratio (LLR) form. The LLR of the *a posteriori* probability is firstly generated based on joint channel estimation and symbol detection (JED) algorithm. The expectation and maximization (EM) is used to solve the optimization problem of JED. This EM-JED algorithm will be introduced in the following Chapter. And the RA decoder can be seen as the differential decoder. In each turbo iteration, a number of inner iterations within LDPC decoder is performed. After a prescribed maximum number of turbo iterations, the LDPC decoder computes the LLR from which the information bits \hat{s} are decided.

Chapter 3

Joint Channel Estimation and Symbol Detection based on EM Algorithm



In the non-coherent fading channels, the EM-JED algorithm is proposed to do both channel tracking and symbol detection. The fading channel coefficients and the transmitted symbols can be modeled as hidden Markov processes. The maximization likelihood (ML) is used to estimate these hidden Markov parameters. However it is difficult to solve this maximization problem. The EM algorithm is an iterative procedure which is suitable for solving the ML problem. The detail is introduced in the following.

3.1 EM-based joint channel estimation and symbol detection in flat fading channels

The received signal y_m is given by

$$y_m = h_m x_m + n_m,$$

where m is the time index.

Based on the autoregressive (AR) model, the fading channel coefficients h_m can be written as

$$h_m = \mathbb{F}\tilde{\mathbf{h}}_{m-1} + BV_m, \quad (3.1)$$

where

$$\tilde{\mathbf{h}}_{m-1} = [h_{m-1}, h_{m-2}, \dots, h_{m-Lh}].$$

The notation of $\underline{\mathbf{x}}_m$, $\underline{\mathbf{h}}_m$, and $\underline{\mathbf{y}}_m$ are shown as

$$\underline{\mathbf{x}}_m = [x_1, x_2, \dots, x_m]^T,$$

$$\underline{\mathbf{h}}_m = [h_1, h_2, \dots, h_m]^T,$$

and

$$\underline{\mathbf{y}}_m = [y_1, y_2, \dots, y_m]^T.$$

Then, the ML estimation of the fading channel coefficients h_m is given by

$$\hat{\underline{\mathbf{h}}}_m = \arg \max_{\underline{\mathbf{h}}_m} \log p(\underline{\mathbf{y}}_m, \underline{\mathbf{h}}_m) = \arg \max_{\underline{\mathbf{h}}_m} \log \sum_{\underline{\mathbf{x}}_m} p(\underline{\mathbf{y}}_m, \underline{\mathbf{h}}_m, \underline{\mathbf{x}}_m).$$

Based on the EM algorithm, it can be written as

$$\begin{aligned}
\hat{\mathbf{h}}_m^l &= \arg \max_{\mathbf{h}_m} \sum_{\mathbf{x}_m} \log p(\underline{y}_m, \mathbf{h}_m, \mathbf{x}_m) p(\mathbf{x}_m | \underline{y}_m, \hat{\mathbf{h}}_m^{l-1}) \\
&= \arg \max_{\mathbf{h}_m} \mathbf{E}_{\mathbf{x}_m} [\log p(\underline{y}_m, \mathbf{h}_m, \mathbf{x}_m) | \underline{y}_m, \hat{\mathbf{h}}_m^{l-1}], \tag{3.2}
\end{aligned}$$

in the l th round of EM iteration.

Define $Q_m(\mathbf{h}_m | \hat{\mathbf{h}}_m^{l-1})$ of the E-step as

$$\begin{aligned}
Q_m(\mathbf{h}_m | \hat{\mathbf{h}}_m^{l-1}) &\triangleq \mathbf{E}_{\mathbf{x}_m} [\log p(\underline{y}_m, \mathbf{h}_m, \mathbf{x}_m) | \underline{y}_m, \hat{\mathbf{h}}_m^{l-1}] \\
&= \mathbf{E}_{\mathbf{x}_m} [\log p(y_m | h_m, x_m) + \log p(x_m) \\
&\quad + \log p(h_m | \tilde{\mathbf{h}}_{m-1}) + \log p(\underline{y}_{m-1}, \mathbf{h}_{m-1}, \mathbf{x}_{m-1}) | \underline{y}_m, \hat{\mathbf{h}}_m^{l-1}] \\
&= Q_m(\mathbf{h}_{m-1} | \hat{\mathbf{h}}_m^{l-1}) + \mathbf{E}_{\mathbf{x}_m} [\log p(x_m) | \underline{y}_m, \hat{\mathbf{h}}_m^{l-1}] \\
&\quad + \mathbf{E}_{\mathbf{x}_m} [\log p(y_m | h_m, x_m) | \underline{y}_m, \hat{\mathbf{h}}_m^{l-1}] + \log p(h_m | \tilde{\mathbf{h}}_{m-1}), \tag{3.3}
\end{aligned}$$

where

$$Q_m(\mathbf{h}_{m-1} | \hat{\mathbf{h}}_m^{l-1}) = \mathbf{E}_{\mathbf{x}_m} [\log p(\underline{y}_{m-1}, \mathbf{h}_{m-1}, \mathbf{x}_{m-1}) | \underline{y}_m, \hat{\mathbf{h}}_m^{l-1}]. \tag{3.4}$$

Then the EM algorithm performs by the iterative procedure as follows

E-step: Compute $Q_m(\mathbf{h}_m | \hat{\mathbf{h}}_m^{l-1})$

M-step: $\hat{\mathbf{h}}_m^l = \arg \max_{\mathbf{h}_m} (Q_m(\mathbf{h}_m | \hat{\mathbf{h}}_m^{l-1}))$

Since $\log p(x_m)$ is constant, $\mathbf{E}_{\mathbf{x}_m} [\log p(x_m) | \underline{y}_m, \hat{\mathbf{h}}_m^{l-1}]$ can be neglected. The other equations are calculated as

$$\mathbf{E}_{\mathbf{x}_m} [\log p(y_m | h_m, x_m) | \underline{y}_m, \hat{\mathbf{h}}_m^{l-1}] \cong -\mathbf{E}_{\mathbf{x}_m} [1/\sigma_n^2 \| y_m - h_m x_m \|^2 | \underline{y}_m, \hat{\mathbf{h}}_m^{l-1}], \tag{3.5}$$

and

$$\log p(h_m | \tilde{\mathbf{h}}_{m-1}) \cong -(h_m - F\tilde{\mathbf{h}}_{m-1})^H (BB^H)^{-1} (h_m - F\tilde{\mathbf{h}}_{m-1}). \quad (3.6)$$

Finally we substitute (3.5) and (3.6) into (3.3) and (3.2), and the M-step becomes

$$\begin{aligned} \hat{\mathbf{h}}_m^l &= \arg \max_{\mathbf{h}_m} (Q_m(\mathbf{h}_m | \hat{\mathbf{h}}_m^{l-1})) \\ &= \arg \max_{\mathbf{h}_m} (Q_m(\mathbf{h}_{m-1} | \hat{\mathbf{h}}_m^{l-1}) - \mathbf{E}_{\mathbf{x}_m} [1/\sigma_n^2 \| y_m - h_m x_m \|^2 | \underline{y}_m, \hat{\mathbf{h}}_m^{l-1}]) \\ &\quad - (h_m - F\tilde{\mathbf{h}}_{m-1})^H (BB^H)^{-1} (h_m - F\tilde{\mathbf{h}}_{m-1})) \\ &= \arg \max_{\mathbf{h}_m} (Q_{m-1}(\mathbf{h}_{m-1} | \hat{\mathbf{h}}_m^{l-1}) + \frac{1}{\sigma^2} [y_m^H h_m \tilde{x}_m + y_m \tilde{x}_m^H h_m^H - \| h_m \|^2 \tilde{\aleph}_m]) \\ &\quad - (h_m - F\tilde{\mathbf{h}}_{m-1})^H (BB^H)^{-1} (h_m - F\tilde{\mathbf{h}}_{m-1})) \end{aligned} \quad (3.7)$$

where \tilde{x}_m and $\tilde{\aleph}_m$ are defined as

$$\tilde{x}_m = \mathbf{E}_{\mathbf{x}_m} [x_m | \underline{y}_m, \hat{\mathbf{h}}_m^{l-1}] \quad (3.8)$$

$$\tilde{\aleph}_m = \mathbf{E}_{\mathbf{x}_m} [\| x_m \|^2 | \underline{y}_m, \hat{\mathbf{h}}_m^{l-1}] \quad (3.9)$$

To solve the M-step $\hat{\mathbf{h}}_m^l = \arg \max_{\mathbf{h}_m} (Q_m(\mathbf{h}_m | \hat{\mathbf{h}}_m^{l-1}))$, we have

$$\frac{\partial Q_m(\mathbf{h}_m | \hat{\mathbf{h}}_m^{l-1})}{\partial \mathbf{h}_m^T} \Big|_{\mathbf{h}_m = \hat{\mathbf{h}}_m^l} = 0 \quad (3.10)$$

Then the Newton-Raphson method is applied and it becomes

$$\hat{\mathbf{h}}_m^l = \left[\frac{\mathbf{F}\hat{\mathbf{h}}_{m-1}^l}{\hat{\mathbf{h}}_{m-1}^l} \right] - \left[\left(\frac{\partial^2 Q_m(\mathbf{h}_m | \hat{\mathbf{h}}_m^{l-1})}{\partial \mathbf{h}_m^* \partial \mathbf{h}_m^T} \right) \Big|_{\mathbf{h}_m = \hat{\mathbf{h}}_m^l} \right]^{-1} \left[\left(\frac{\partial Q_m(\mathbf{h}_m | \hat{\mathbf{h}}_m^{l-1})}{\partial \mathbf{h}_m^T} \right) \Big|_{\mathbf{h}_m = \hat{\mathbf{h}}_m^l} \right], \quad (3.11)$$

where h_m is as shown in (3.1), and

$$\dot{\mathbf{h}}_m = [\mathbf{F}\hat{\mathbf{h}}_{m-1}^l, \hat{\mathbf{h}}_{m-1}^l]^T.$$

To obtain $[(\frac{\partial Q_m(\underline{\mathbf{h}}_m | \hat{\underline{\mathbf{h}}}_m^{l-1})}{\partial \underline{\mathbf{h}}_m^T}) |_{\underline{\mathbf{h}}_m = \hat{\underline{\mathbf{h}}}_m}]$, we have

$$[(\frac{\partial Q_m(\underline{\mathbf{h}}_m | \hat{\underline{\mathbf{h}}}_m^{l-1})}{\partial \underline{\mathbf{h}}_m^T}) |_{\underline{\mathbf{h}}_m = \hat{\underline{\mathbf{h}}}_m}] = \frac{1}{\sigma_n^2} [\frac{1}{\underline{\mathbf{0}}}] [\tilde{x}_m y_m^* - \tilde{\mathfrak{K}}_m(\underline{\mathbf{F}} \hat{\underline{\mathbf{h}}}_{m-1}^l)^*] \quad (3.12)$$

To obtain $[(\frac{\partial^2 Q_m(\underline{\mathbf{h}}_m | \hat{\underline{\mathbf{h}}}_m^{l-1})}{\partial \underline{\mathbf{h}}_m^* \partial \underline{\mathbf{h}}_m^T}) |_{\underline{\mathbf{h}}_m = \hat{\underline{\mathbf{h}}}_m}]$, we have

$$\begin{aligned} [(\frac{\partial^2 Q_m(\underline{\mathbf{h}}_m | \hat{\underline{\mathbf{h}}}_m^{l-1})}{\partial \underline{\mathbf{h}}_m^* \partial \underline{\mathbf{h}}_m^T}) |_{\underline{\mathbf{h}}_m = \hat{\underline{\mathbf{h}}}_m}] &= [(\frac{\partial^2 Q_m(\underline{\mathbf{h}}_{m-1} | \hat{\underline{\mathbf{h}}}_m^{l-1})}{\partial \underline{\mathbf{h}}_m^* \partial \underline{\mathbf{h}}_m^T})] \\ &\quad - [\frac{1}{-\underline{\mathbf{F}}^T}] (B^* B)^{-1} [1 | -\underline{\mathbf{F}}^*] + \frac{1}{\sigma_n^2} [\frac{1}{\underline{\mathbf{0}}}] \tilde{\mathfrak{K}}_m [1 | \underline{\mathbf{0}}] \end{aligned} \quad (3.13)$$

Besides, we define

$$-\underline{\mathbf{P}}_m^{-1} \triangleq (\frac{\partial^2 Q_m(\underline{\mathbf{h}}_m | \hat{\underline{\mathbf{h}}}_m^{l-1})}{\partial \underline{\mathbf{h}}_m^* \partial \underline{\mathbf{h}}_m^T}),$$

and the upper-left $L_h \times L_h$ submatrix of $(\underline{\mathbf{P}}_m^{-1})$ as $(\underline{\mathbf{P}}_m^{-1})_{L_h \times L_h}$, where

$$[(\frac{\partial^2 Q_m(\underline{\mathbf{h}}_{m-1} | \hat{\underline{\mathbf{h}}}_m^{l-1})}{\partial \underline{\mathbf{h}}_m^* \partial \underline{\mathbf{h}}_m^T})] = \begin{bmatrix} 0 & \underline{\mathbf{0}} \\ \underline{\mathbf{0}} & -(\underline{\mathbf{P}}_{m-1}^{-1})_{L_h \times L_h} \end{bmatrix}.$$

We also define

$$\begin{aligned}
-P_{m|m-1}^{-1} &= \frac{\partial^2 Q_m(\underline{h}_{m-1} | \hat{h}_m^{l-1})}{\partial \underline{h}_m^* \partial \underline{h}_m^T} - \left[\frac{1}{-\underline{\mathbb{F}}^T} \right] (B^* B)^{-1} [1 | -\underline{\mathbb{F}}^*] \\
P_{m|m-1} &= \begin{bmatrix} 0 & \underline{\mathbb{0}} \\ \underline{\mathbb{0}} & (\underline{\mathbb{P}}_{m-1}^{-1})_{L_h \times L_h} \end{bmatrix} + \left[\frac{1}{-\underline{\mathbb{F}}^T} \right] (B^* B)^{-1} [1 | -\underline{\mathbb{F}}^*]^{-1} \\
&= \begin{bmatrix} (B^* B)^{-1} & -(B^* B)^{-1} \underline{\mathbb{F}}^* \\ -\underline{\mathbb{F}}^T (B^* B)^{-1} & (\underline{\mathbb{P}}_{m-1}^{-1})_{L_h \times L_h} + \underline{\mathbb{F}}^T (B^* B)^{-1} \underline{\mathbb{F}}^* \end{bmatrix}^{-1} \\
&= \begin{bmatrix} BB^* + \underline{\mathbb{F}}^* \underline{\mathbb{P}}_{m-1} \underline{\mathbb{F}}^T & \underline{\mathbb{F}}^* \underline{\mathbb{P}}_{m-1} \\ \underline{\mathbb{P}}_{m-1} \underline{\mathbb{F}}^T & \underline{\mathbb{P}}_{m-1} \end{bmatrix}. \tag{3.14}
\end{aligned}$$

The above equation (3.14) is computed by matrix inversion lemma. Finally, it becomes

$$\begin{aligned}
\underline{\mathbb{P}}_m &= (\underline{\mathbb{P}}_{m|m-1}^{-1} + \frac{1}{\sigma_n^2} \left[\frac{1}{\underline{\mathbb{0}}} \right] \tilde{\aleph}_n [1 | \underline{\mathbb{0}}])^{-1} \\
&= P_{m|m-1} - P_{m|m-1} \begin{bmatrix} J \\ \underline{\mathbb{0}} \end{bmatrix} [\sigma_n^2 + [J^H | \underline{\mathbb{0}}] P_{m|m-1} \begin{bmatrix} J \\ \underline{\mathbb{0}} \end{bmatrix}]^{-1} [J^H | \underline{\mathbb{0}}] P_{m|m-1} \\
&= P_{m|m-1} - \left[\frac{BB^* + \underline{\mathbb{F}}^* \underline{\mathbb{P}}_{m-1} \underline{\mathbb{F}}^T}{\underline{\mathbb{P}}_{m-1} \underline{\mathbb{F}}^T} \right] J (\sigma_n^2 + J^H (BB^* + \underline{\mathbb{F}}^* \underline{\mathbb{P}}_{m-1} \underline{\mathbb{F}}^T) J)^{-1} \\
&\times J^H [BB^* + \underline{\mathbb{F}}^* \underline{\mathbb{P}}_{m-1} \underline{\mathbb{F}}^T | \underline{\mathbb{F}}^* \underline{\mathbb{P}}_{m-1}], \tag{3.15}
\end{aligned}$$

where $\tilde{\aleph}_n$ is positive definite and $\tilde{\aleph}_n = JJ^H$. By substituting (3.12) and (3.15) into (3.11), we finally have

$$\begin{aligned}
\hat{h}_m^l &= \left[\frac{\underline{\mathbb{F}} \hat{h}_{m-1}^l}{\hat{h}_{m-1}^l} \right] + \left[\frac{BB^* + \underline{\mathbb{F}} \underline{\mathbb{P}}_{m-1} \underline{\mathbb{F}}^T}{\underline{\mathbb{P}}_{m-1} \underline{\mathbb{F}}^T} \right] \\
&\times [1 - J[\sigma_n^2 + J^H (BB^* + \underline{\mathbb{F}}^* \underline{\mathbb{P}}_{m-1} \underline{\mathbb{F}}^T) J]^{-1} J^H (BB^* + \underline{\mathbb{F}}^* \underline{\mathbb{P}}_{m-1} \underline{\mathbb{F}}^T)] \\
&\times \frac{1}{\sigma_n^2} [\tilde{x}_m y_m^* - \tilde{\aleph}_m (\underline{\mathbb{F}} \hat{h}_{m-1}^l)^*] \tag{3.16}
\end{aligned}$$

The joint channel estimation and symbol detection algorithm is summarized as follows. Starting from some initial value \hat{h}_1^0 , where $l=0$ and $m=1$. The EM algorithm is iteratively solved for l times. For instance, the procedure of JED algorithm for m th received signal is explained.

Step 1 : In flat-fading channels, the fading channel coefficients are correlated with each other in the same coherence interval. So we take \hat{h}_{m-1}^ℓ as the initial value of \hat{h}_m^0 .

Step 2 : \tilde{x}_m and $\tilde{\mathfrak{N}}_m$ are calculated by the fact that

$$p(x_m | \underline{y}_m, \hat{\underline{h}}_m^{\ell-1}) \propto p(\underline{y}_m | x_m, \hat{\underline{h}}_m^{\ell-1})$$

Step 3 : \hat{h}_m^ℓ is then computed by (3.16). And return to step2 with the updated \hat{h}_m^ℓ .

The stable value of \hat{h}_m^ℓ is obtained by the iterative procedure between step 2 and step 3 for l times.

Step 4 : For the next $(m + 1)$ th received signal, \hat{h}_m^ℓ is taken as the initial value of \hat{h}_{m+1}^0 and \underline{P}_m is also updated by (3.15). As in the step 2, \tilde{x}_{m+1} and $\tilde{\mathfrak{N}}_{m+1}$ are computed.

Step 5 : \hat{h}_{m+1}^ℓ is similarly computed by (3.16).

Step 6 : Repeat the step 4 and step 5 iteratively for each signal.

The above procedure of JED algorithm is also shown in Fig. 3.1.

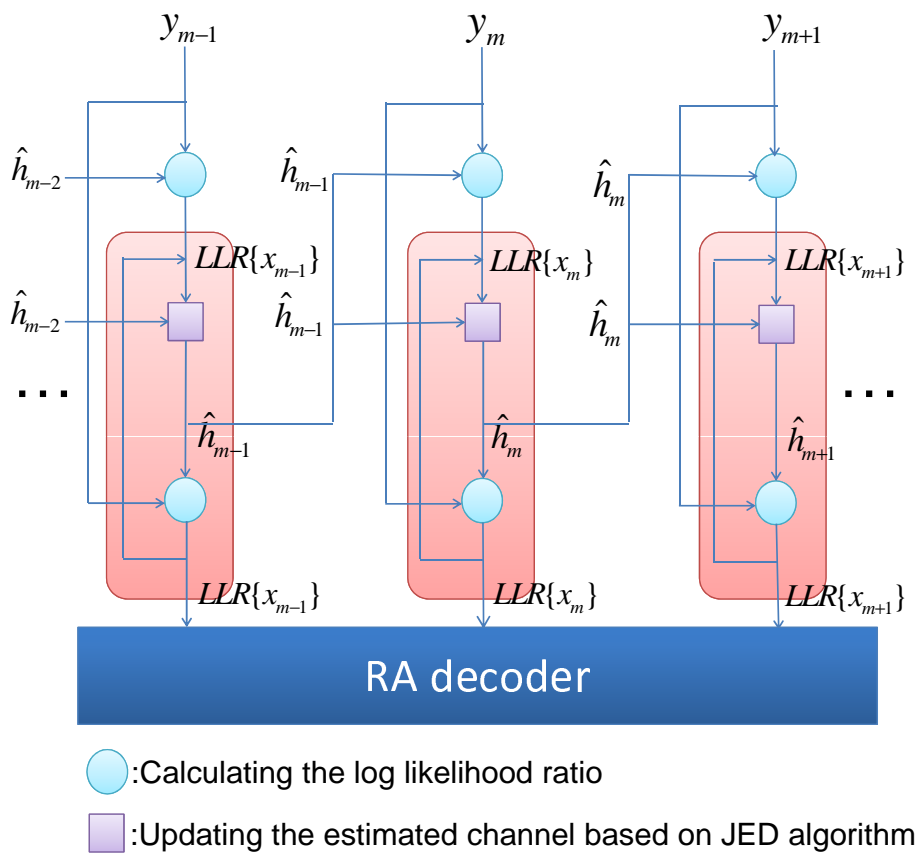


Figure 3.1: Illustration of JED algorithm.

Chapter 4

RA Decoder

The RA decoder, seen as the differential decoder, is connected to the EM-JED algorithm and LDPC decoder. The RA code here serves as the inner code and the LDPC code serves as the outer code of a serially concatenated turbo-like code. Besides, the RA code is used to solve the phase ambiguities associated with the channel estimates obtained with the EM-JED algorithm. The phase ambiguities are shown in Fig. 4.1.

Besides, the differential encoder can be seen as the combination of both variable nodes and check nodes. Hence the RA encoder here is presented as some kind of Tanner graph which contains both variable nodes and check nodes in Fig. 4.2. The conventional BCJR algorithm, used as the differential decoder, can be referred to [22]. The RA decoder here is modified with the extrinsic message computation of message passing algorithm (MPA) at variable nodes and check nodes as in the LDPC code. This kind of RA decoder helps us in adding some design criteria of LDPC codes shown in the next chapter.

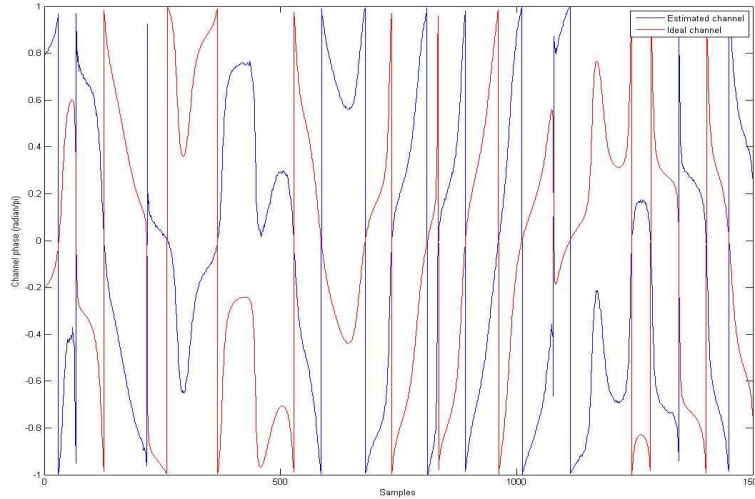


Figure 4.1: The phase ambiguities associated with the channel estimates obtained with the EM-JED algorithm.

4.1 Design Criteria of LDPC Code

Since the RA encoder is presented as some kind of Tanner graph in Fig. 4.2, the transmitter of both LDPC encoder and RA encoder can be also shown with the Tanner graph in Fig. 4.3. In Fig. 4.3, two classes of short cycles are both shown. One is the shortest possible cycle in LDPC code denoted by four bold blue edges in the figure. The other is the short length cycle constituted by both LDPC code and differential encoder exemplified by five bold green edges. One thing to be noted is that this kind of short cycles can be much easily detected without the interleaver added between the LDPC encoder and the RA encoder. Hence it should be avoided the adjacent variable nodes connected to the same check node. In fading channels, the dependence of variable nodes lingers slightly for the correlated fading channel coefficients. Therefore the variable nodes connected to the same check node are also restricted to be in different coherence intervals (The coherence interval here is assumed to be the inverse of the fading speed.) to satisfy the independence assumption for the cycle-free condition of LDPC code.

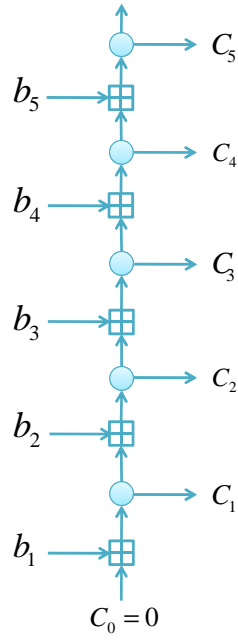


Figure 4.2: The RA encoder associated with the Tanner graph.

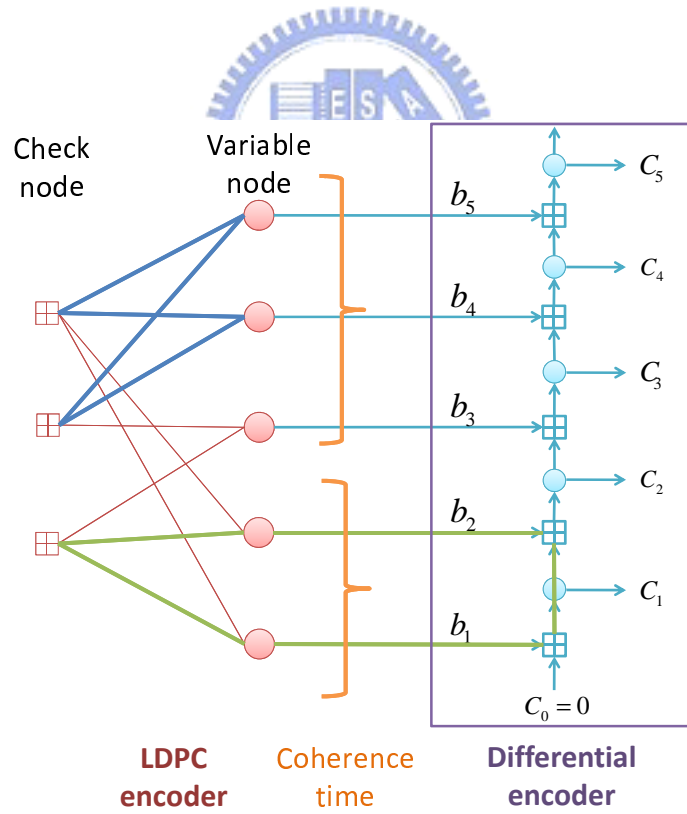


Figure 4.3: The Tanner graph of both LDPC encoder and RA encoder.

The design criteria are summarized as follows:

- Eliminating length-4 cycles in LDPC code.
- Preventing adjacent variable nodes from connecting to the same check node to avoid short cycles appearing in the concatenated LDPC and RA code.
- The variable nodes connected to the same check node should be in different coherence intervals to meet the independence assumption for the cycle-free condition of LDPC. (The coherence time here is assumed to be the inverse of the fading speed.)

The fastest fading speed in our simulation results is 0.01. Therefore if the last design criterion is fulfilled, the second design criterion is always satisfied. We compare the performance of regular (3,6) degree profile with and without the last criterion in Fig. 4.4. The difference of these two performance curves occurs at high SNR region. Besides, the ideal fading channel means that the fading channel coefficients are perfectly known at the receiver.



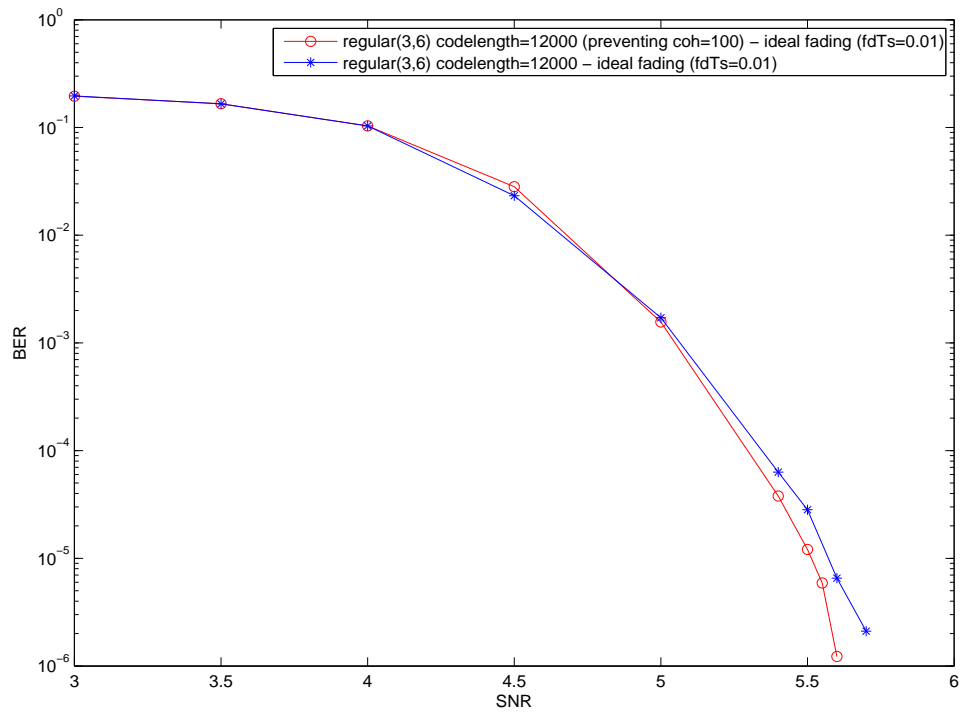


Figure 4.4: The performance of the regular (3,6) degree profile and codeword length 12000 in ideal fading channel.

Chapter 5

Combined EM-JED algorithm and LDPC Decoding

In this chapter, the message passing algorithm (MPA) of LDPC code is briefly introduced. The MPA is also known as sum-product algorithm (SPA) and belief propagation algorithm (BPA). In last section, the procedure of computing extrinsic information in each block of the turbo-like iterative receiver is summarized.

5.1 LDPC Decoding

Low density parity check (LDPC) codes were firstly proposed by Gallager in 1960 [3]. LDPC code is a linear block code which provides capacity-approaching performance. The LDPC code is scarcely used until the mid-1990's. The study of LDPC codes is rediscovered for its near-capacity performance. The Tanner graph of LDPC code is used to described the decoding algorithm of MPA based on the given parity check matrix H . By iteratively computing the *a posteriori* probability (APP) of the transmitted codeword conditioned on the received word in each variable node and check node, the reliability of the APPs can be improved after a number of LDPC iterations.

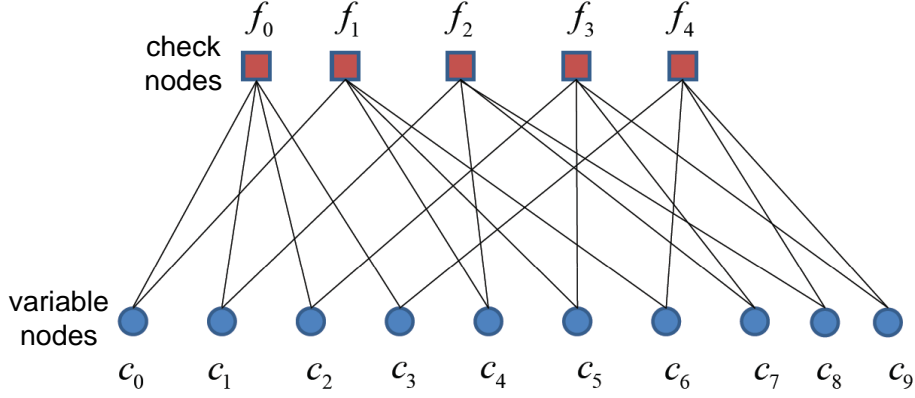


Figure 5.1: Tanner graph of LDPC code.

5.1.1 Variable Nodes Analysis

Like finding the maximum *a posteriori* (MAP) in other trellis decoder, the APPs are also considered in LDPC decoder. The APP is computed by the probability of a given bit in the transmitted codeword $\mathbf{c} = [c_0, c_1, \dots, c_{n-1}]$ that equals 1 or 0 conditioned on the received word $\mathbf{y} = [y_0, y_1, \dots, y_{n-1}]$. The computation is extended to log-APP ratio in general use, also known as log-likelihood ratio (LLR):

$$L(c_i) \triangleq \log \left(\frac{\Pr(c_i = 0 | \mathbf{y})}{\Pr(c_i = 1 | \mathbf{y})} \right)$$

The half-iteration message passing of variable node c_i is shown in Fig. 5.2. The extrinsic message $q_{ij}(b)$ serves as the APP along the edge passed from variable node c_i to check node f_j . The prior message r_{ji} denotes the APP along the edge passed from other check nodes except f_j to the variable node c_i . Hence the computation of the extrinsic LLR $L(q_{ij})$ is written as

$$L(q_{ij}) = L(c_i) + \sum_{j' \in C_i \setminus j} L(r_{j'i}), \quad (5.1)$$

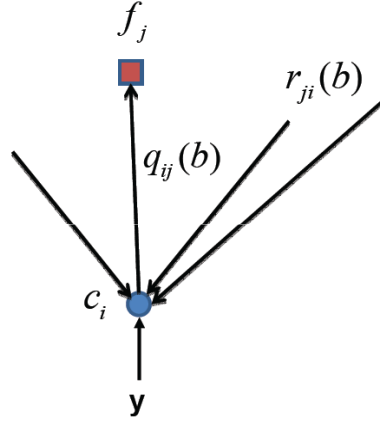


Figure 5.2: The computation of extrinsic message q_{ij} at the variable node c_i .

where $L(c_i)$ is the prior LLRs sent into LDPC decoder.

5.1.2 Check Nodes Analysis

The half-iteration message passing of check node f_j is shown in Fig. 5.3. The extrinsic message $r_{ji}(b)$ is observed by the sum modulo-2 of prior message q_{ij} . The computation of the extrinsic LLR $L(r_{ji})$ is written as

$$L(r_{ij}) = (\prod_{i' \in V_j \setminus i} \alpha_{i'}) \times (\phi(\sum_{i' \in V_j \setminus i} \beta_{i'})), \quad (5.2)$$

where $\alpha = \mathbf{sign}|L(q_{ij})|$, $\beta = |L(q_{ij})|$, and $\phi(x) = \log(\frac{e^x+1}{e^x-1})$.

5.2 Combined EM-JED algorithm and RA decoder with LDPC Decoding

The turbo-like iterative receiver can be seen as three connected blocks in Fig. 5.4. The extrinsic message is iteratively passed between each block. The computation of the

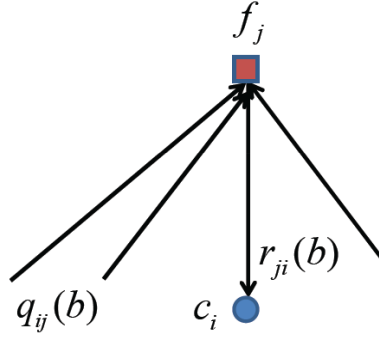


Figure 5.3: The computation of extrinsic message r_{ji} at the check node f_j .

extrinsic LLRs of each block is summarized as follows.

- Step1: In the initialization, the extrinsic LLRs L_F and L_D are set zero.
- Step2: With the received signal y and the prior information L_F passed from RA decoder, the fading channel coefficients are estimated based on EM-JED algorithm. And the extrinsic LLRs L_B is then computed by both the estimated channel coefficients and the received signal.
- Step3: The RA decoder here is combined with the conventional forward-backward algorithm of BCJR and the graph-based RA code in Fig. 4.2. The forward and the backward probabilities or LLRs are computed by the prior information L_B and L_D . The output extrinsic LLRs L_C is then computed with forward, backward LLRs and the prior information L_B passed from EM-JED algorithm referred to Fig. 4.2.
- Step4: The prior information L_C is sent into the LDPC decoder. After the number of LDPC iterations, the extrinsic LLRs L_D are passed back to the RA decoder.
- Step5: Similar to step3, the forward and backward LLRs are computed by the prior information L_B and L_D . The output extrinsic LLRs L_F is then computed with forward , backward LLRs and the prior information L_D passed from LDPC decoder.

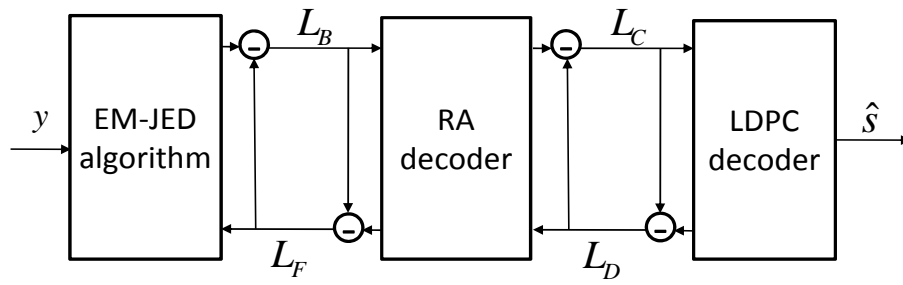


Figure 5.4: Illustration of the iterative procedure in the receiver.

The extrinsic messages are then iteratively passed between each block in the receiver with the step2, step3, step4 and step5.



Chapter 6

Density Evolution

The density evolution is used to find the limits of performance of combined EM-JED algorithm and LDPC decoding. The density evolution with Gaussian approximation in [21] is summarized here for reference. Firstly, the output log-likelihood ratios (LLRs) passed from EM-JED algorithm and RA decoder to LDPC decoder are generated by Monte Carlo simulation. Then the probability density function (pdf) of these output LLRs is modeled as a mixture of symmetric Gaussians based on the EM algorithm. With the assumption of the symmetric Gaussian mixtures of the output LLRs, the evolution of the pdfs can be easily tracked through message-passing algorithm within LDPC decoder. The pdf of the output extrinsic messages of the variable nodes would become symmetric Gaussian mixtures due to both the irregularity of variable degree and the pdf of the output LLRs of RA decoder. Similarly the pdf of the output extrinsic messages of the check nodes is affected by the irregularity of the check degree. To reduce the complexity of computing the pdf of the output extrinsic messages of the check nodes, we only consider the check-regular degree profile here. With only check-regular degree profile considered, there still occurs some differences in the histogram of variable-regular degree profile and variable-irregular degree profile. The histogram is shown in the sequel. In [21], the pdf of the output extrinsic messages of the check nodes is assumed Gaussian

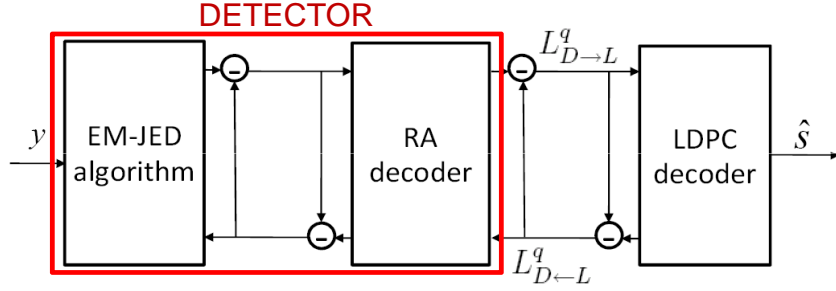


Figure 6.1: Illustration of density evolution of the iterative receiver.

distributed. Nevertheless, it has not been suitable to make Gaussian approximation of the output extrinsic messages of the check nodes with variable-irregular degree profile. However, the density evolution with Gaussian approximation would become much easier by only tracking the mean of the pdfs within the LDPC decoder.



The procedure of computing the pdfs of the extrinsic LLRs of LDPC decoding is described as follows. The subscript $D \rightarrow L$ denotes quantities sent from the EM-JED algorithm and RA decoder to LDPC decoder and vice versa, $D \leftarrow L$. Here the subscript D denotes the DETECTOR which contains both the EM-JED algorithm and RA decoder. The subscript $b \rightarrow c$ denotes quantities sent from variable nodes to check nodes and vice versa, $b \leftarrow c$. The superscript p denotes p th iteration time of LDPC decoder. And the superscript q denotes the q th iteration time of the overall iterative receiver. The superscript $d_{l,max}$ denotes the maximum variable degree and $d_{r,max}$ denotes the maximum check degree.

- Initialization:

- Set $f_{b \leftarrow c}^{0,0}(x) = \delta(x)$ and $f_{D \leftarrow L}^0(x) = \delta(x)$.

- Turbo iterations of receiver: ($q = 1, 2, \dots, Q$)
 - In the fading channel, the pdf of the extrinsic messages passed from DETECTOR to LDPC decoder is modeled as symmetric Gaussian mixtures based on the EM algorithm. The details can be referred to [21]. Hence, the pdfs of the extrinsic messages passed from DETECTOR are computed as

$$f_{D \rightarrow L}^q = \sum_{j=1}^J \pi_j \mathcal{N}(\mu_j, 2\mu_j), \quad (6.1)$$

where J is the number of Gaussian component.

- Computing the pdf of the extrinsic messages within LDPC iteration. ($p = 1, 2, \dots, P$)
 - * At a variable node of degree i :

The pdf of the extrinsic messages passed along an edge from variable node of degree i is denoted by $f_{b \rightarrow c, i}^{p, q}$ and it is computed by the convolution of $f_{D \rightarrow L}^q$ with $(i - 1)$ convolutions of $f_{b \leftarrow c}^{p-1, q}$.

$$f_{b \rightarrow c, i}^{p, q} = f_{D \rightarrow L}^q \otimes \underbrace{f_{b \leftarrow c}^{p-1, q} \otimes f_{b \leftarrow c}^{p-1, q} \otimes \dots \otimes f_{b \leftarrow c}^{p-1, q}}_{(i-1) \text{ convolutions}} \quad (6.2)$$

- If $f_{b \leftarrow c}^{p-1, q}$ is assumed Gaussian distributed, it means that

$$f_{b \leftarrow c}^{p-1, q} = \mathcal{N}(m_{b \leftarrow c}^{p-1, q}, 2m_{b \leftarrow c}^{p-1, q})$$

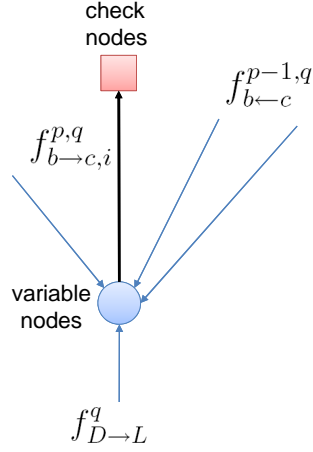


Figure 6.2: Illustration of half-iteration message passing at variable node in density evolution.

Hence,

$$\begin{aligned}
 f_{b \rightarrow c, i}^{p, q} &= f_{D \rightarrow L}^q \otimes \mathcal{N}((i-1)m_{b \leftarrow c}^{p-1, q}, 2(i-1)m_{b \leftarrow c}^{p-1, q}) \\
 &= \left(\sum_{j=1}^J \pi_j \mathcal{N}(\mu_j, 2\mu_j) \right) \otimes \mathcal{N}((i-1)m_{b \leftarrow c}^{p-1, q}, 2(i-1)m_{b \leftarrow c}^{p-1, q}) \quad (6.3) \\
 &= \sum_{j=1}^J \pi_j \mathcal{N}(\mu_j + (i-1)m_{b \leftarrow c}^{p-1, q}, 2[\mu_j + (i-1)m_{b \leftarrow c}^{p-1, q}])
 \end{aligned}$$

- * The pdf of the extrinsic messages passed from the variable nodes to the check nodes along an edge:

$$f_{b \rightarrow c}^{p, q} = \sum_{i=2}^{d_{l, max}} \lambda_i f_{b \rightarrow c, i}^{p, q} \quad (6.4)$$

(λ_i : fractions of the edges connected to variable nodes of degree i)

- * At a check node of degree l : The computation of the tanh rule at the check nodes is shown as

$$\tanh\left(\frac{L_{b \leftarrow c}^{p, q}(e_r)}{2}\right) = \prod_{k=1, k \neq r}^l \tanh\left(\frac{L_{b \leftarrow c}^{p, q}(e_k)}{2}\right). \quad (6.5)$$

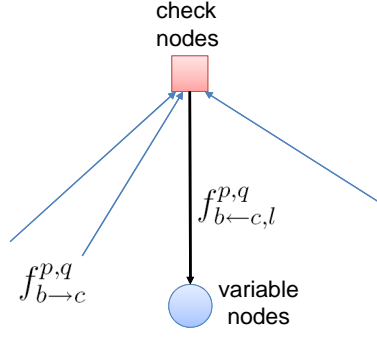


Figure 6.3: Illustration of half-iteration message passing at check node in density evolution.

- If $f_{b←c}^{p,q}$ is assumed Gaussian distributed, we can firstly take the expectation of both sides in (6.5) and it becomes

$$E \left\{ \tanh\left(\frac{L_{b←c}^{p,q}(e_r)}{2}\right) \right\} = E \left\{ \left[\prod_{k=1, k \neq r}^l \tanh\left(\frac{L_{b→c}^{p,q}(e_k)}{2}\right) \right] \right\} \quad (6.6)$$

$$= \left[E \left\{ \tanh\left(\frac{L_{b→c}^{p,q}(e_k)}{2}\right) \right\} \right]^{l-1},$$

where $L_{b→c}^{p,q}(e_s)$ and $L_{b→c}^{p,q}(e_k)$ are identically distributed and independent for $k \neq s$.

Denote $\psi(x) \triangleq E \left\{ \tanh\left(\frac{L}{2}\right) \right\}$, where $L \sim \mathcal{N}(x, 2x)$.

Taking the definition of ψ function and (6.3), the equation becomes

$$\psi(m_{b←c,l}^{p,q}) = \left[\sum_{j=1}^J \sum_{i=2}^{d_{l,max}} \pi_j \lambda_i \psi(\mu_j + (i-1)m_{b←c}^{p-1,q}) \right]^{l-1} \quad (6.7)$$

$$= \left[\sum_{j=1}^J \sum_{i=2}^{d_{l,max}} \pi_j \lambda_i \psi(m_{b→c,i,j}^{p,q}) \right]^{l-1}$$

Hence,

$$m_{b←c,l}^{p,q} = \psi^{-1} \left[\left(\sum_{j=1}^J \sum_{i=2}^{d_{l,max}} \pi_j \lambda_i \psi(m_{b→c,i,j}^{p,q}) \right)^{l-1} \right] \quad (6.8)$$

Finally, $f_{b \leftarrow c, l}^{p, q} = \mathcal{N}(m_{b \leftarrow c, l}^{p, q}, 2m_{b \leftarrow c, l}^{p, q})$.

- * The pdf of the extrinsic messages passed from the check nodes to the variable nodes:

$$f_{b \leftarrow c}^{p, q} = \sum_{l=2}^{d_{r, max}} \rho_l f_{b \leftarrow c, l}^{p, q} \quad (6.9)$$

(ρ_l : fractions of the edges connected to check nodes of degree l)

- * Messages passed back to the DETECTOR at a variable node of degree i :
The pdf of the extrinsic messages passed along an edge from variable node of degree i back to the DETECTOR is denoted by $f_{D \leftarrow L, i}^q$ and it is computed by i convolutions of $f_{b \leftarrow c}^{p, q}$.

$$f_{D \leftarrow L, i}^q = \underbrace{f_{b \leftarrow c}^{p, q} \otimes f_{b \leftarrow c}^{p, q} \otimes \dots \otimes f_{b \leftarrow c}^{p, q}}_{i \text{ convolutions}} \quad (6.10)$$

- If $f_{b \leftarrow c}^{p, q}$ is assumed Gaussian distributed, it becomes

$$f_{D \leftarrow L, i}^q = \mathcal{N}(im_{b \leftarrow c}^{p, q}, 2im_{b \leftarrow c}^{p, q}). \quad (6.11)$$

- * Message passed back to the DETECTOR:

$$f_{D \leftarrow L}^q = \sum_{i=2}^{d_{r, max}} \tilde{\lambda}_i f_{D \leftarrow L, i}^q \quad (6.12)$$

($\tilde{\lambda}_i$: fractions of the variable nodes of degree i)

- Finding the minimum SNR:

1. With Gaussian approximation of the pdf of the extrinsic messages passed from check nodes to variable nodes, find the minimum SNR at which $m_{D \leftarrow L}^Q$ or $m_{b \leftarrow c}^{P, Q}$ tends to ∞ .

2. Find the minimum SNR at which the residual error $\int_{-\infty}^0 f^q(z) dz$ tends to zero, where $f_i^q = f_{D \leftarrow L, i}^q \otimes f_{D \rightarrow L}$ and $f^q = \sum_{i=2}^{d_r, \max} \tilde{\lambda}_i f_i^q$.

Obviously, the density evolution becomes much easier with the Gaussian approximation. Considering the check-regular degree profiles, we show the histograms of LLRs passed from check nodes to variable nodes with variable-regular degree profile in Fig. 6.4 and variable-irregular degree profile in Fig. 6.5. Hence, we find that Gaussian approximation can work well at the output extrinsic messages of check nodes with variable-regular degree profile but might fail with the irregular-variable degree profile.



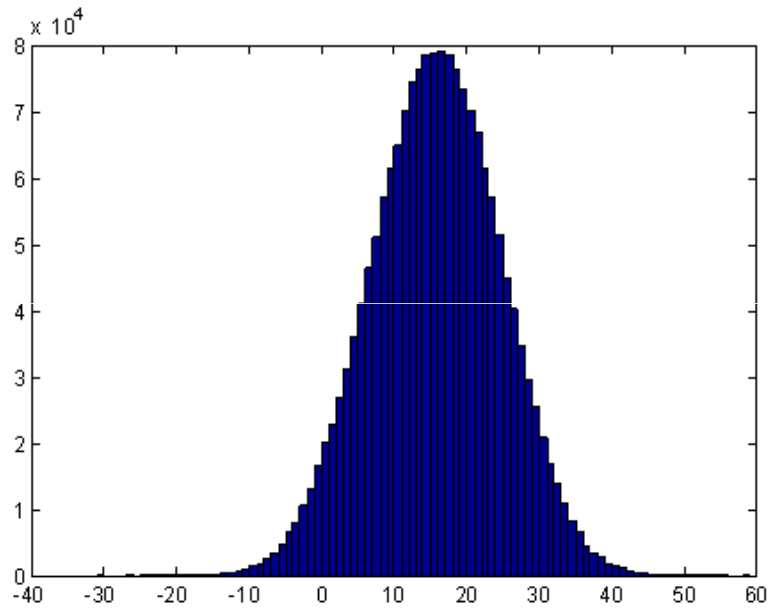


Figure 6.4: The histogram of output LLRs passed from check nodes to variable nodes with regular (3,6) degree profile.

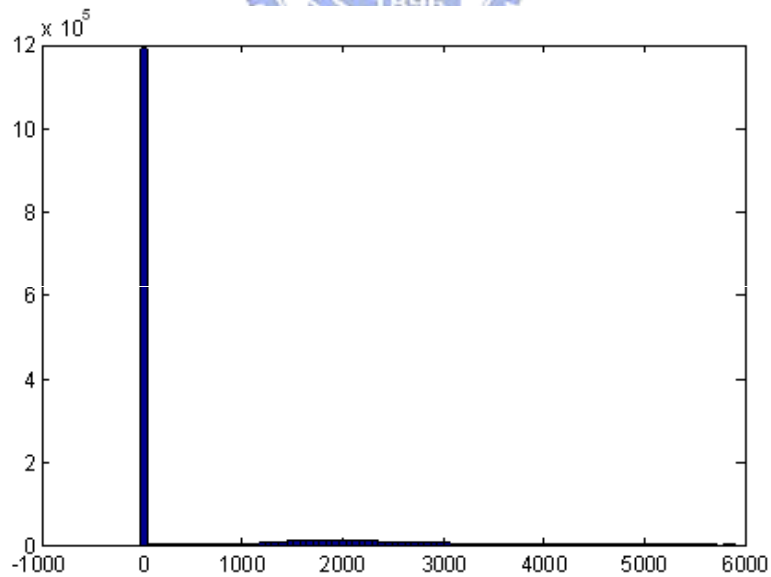


Figure 6.5: The histogram of output LLRs passed from check nodes to variable nodes with variable-irregular and check-regular degree profile.

Chapter 7

EXIT Chart Analysis

The extrinsic information transfer (EXIT) chart is used to predict the performance of iteratively-decoded error-correcting codes, such as LDPC codes and Turbo codes. Divide the iterative receiver into two segments. These two segments of the iterative receiver exchange messages with each other. Instead of tracking the pdfs of the exchanged messages, we track the mutual information between the message and the codeword. In each segment, we can derive its transfer functions of the mutual information. Hence, the iterative message passing can be plotted by these two transfer functions in the EXIT chart.

Here we divide our iterative receiver into two segments. One is the combined DETECTOR and the variable nodes of LDPC code. The other is the check nodes of LDPC code. The EXIT chart analysis in [16] is summarized for reference. Besides, the prior information is assumed symmetric Gaussian distributed in the Appendix of [16] summarized as follows.

Consider $Y = X + N$, where $Pr(X = \pm 1) = \frac{1}{2}$ and N is zero-mean, Gaussian noise with variance σ_n^2 . The LLR $L_{ch}(Y)$ conditioned on $X = \pm 1$ is Gaussian with mean

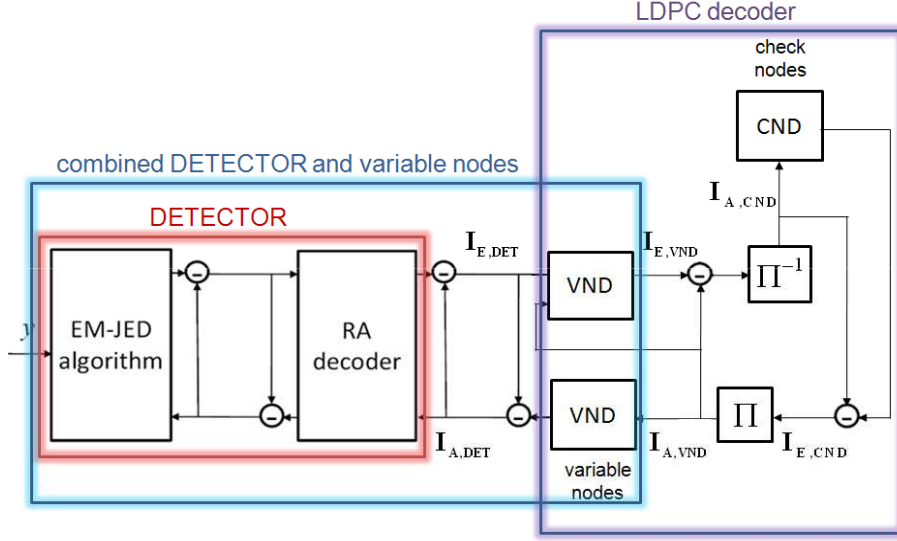
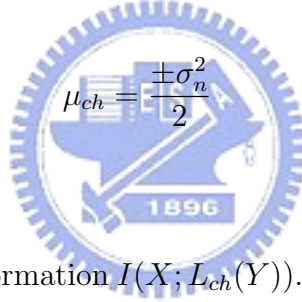


Figure 7.1: Illustration of density evolution of the iterative receiver.

$\mu_{ch} = \frac{\pm 2}{\sigma_n^2}$ and variance $\sigma_{ch}^2 = \frac{4}{\sigma_n^2}$. That means



Define $J(\sigma_{ch})$ be the mutual information $I(X; L_{ch}(Y))$. The definition of $\sigma_A = J^{-1}(I_A)$ is based on the symmetric Gaussian approximation of the prior information. Hence it might also suffer the same problem mentioned above. The symmetric Gaussian approximation might be not always suitable for every degree profile.

The procedure of computing the EXIT curves of the extrinsic LLRs of LDPC decoding is described as follows.

- Step1: Use Monte Carlo simulation to measure the EXIT curve of DETECTOR as

$$I_{E,DET}(I_{A,DET}, SNR), \quad (7.1)$$

where $I_{A,DET} = J(\sigma_A)$ and

$$I_{E,DET} = \frac{1}{2} \sum_{x=+1,-1} \int_{-\infty}^{+\infty} P_E(\zeta | X = x) \cdot \log_2 \frac{2 \cdot P_E(\zeta | X = x)}{P_E(\zeta | X = -1) + P_E(\zeta | X = +1)} d\zeta$$

- Step2: The EXIT curve of both DETECTOR and variable nodes is shown as

– The relationship of $I_{A,DET}$ and $I_{A,VND}$ is showed as

$$I_{A,DET} = J(\sqrt{d_v} \cdot J^{-1}(I_{A,VND})) \quad (7.2)$$

– Hence the EXIT function of combined DETECTOR and variable nodes is showed as

$$I_{E,VND} = J(\sqrt{(d_v - 1)[J^{-1}(I_{A,VND})]^2 + [J^{-1}(I_{E,DET})]^2}), \quad (7.3)$$

where d_v denotes the variable degree.

- Step3: Measure the EXIT curve of check nodes by

$$I_{E,CND} = 1 - \sum_{i=2}^{d_{r,max}} b_i \cdot J(\sqrt{d_{c,i} - 1} \cdot J^{-1}(1 - I_{A,CND})), \quad (7.4)$$

where

$d_{c,i}$: check degree i

b_i : the fraction of the edges connected to the check nodes of degree $d_{c,i}$

- Step4: The EXIT curves are iteratively measured by (7.1), (7.2), (7.3), and (7.4).

Chapter 8

Simulation Results

8.1 Performance of EM-JED algorithm in different fading speeds

The performance of employing the EM-JED algorithm and RA decoder is shown in Fig. 8.1-8.4. Here the differential code is necessary for solving the phase ambiguities associated with the channel estimates obtained with EM-JED algorithm. We measure the performance of the output message of combined EM-JED algorithm and RA decoder in different fading speeds.

From the simulation results, the performance gap between fading channel (noncoherent detection) and ideal fading channel (coherent detection which means that the fading channel coefficients are perfectly known in the receiver) becomes smaller in slower fading speed. It seems that the EM-JED algorithm works better in slower fading speed. In the fading speed 0.01, the performance curve in fading channel becomes much close to the one with perfectly known fading channel coefficients. In Fig. 8.4, the performance curves of coherent detection in different fading speeds are very close.

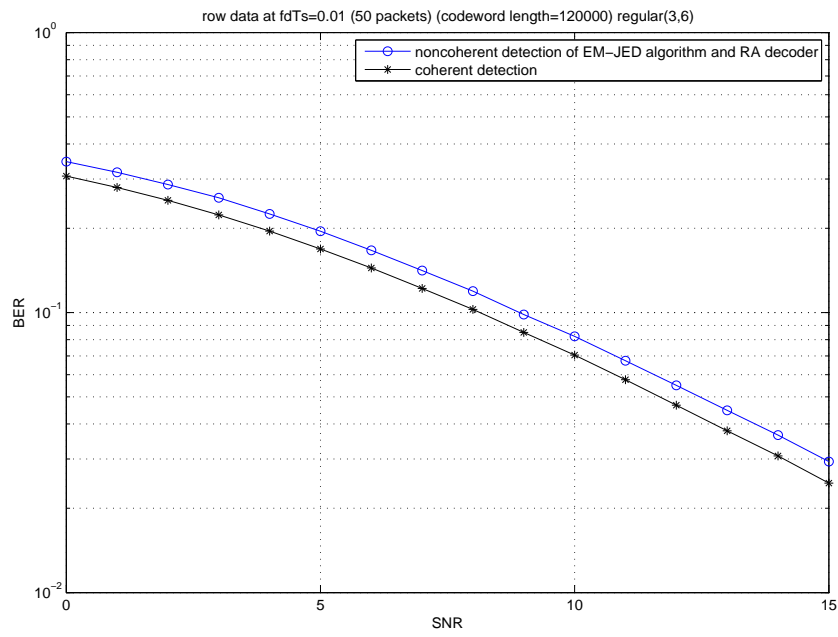


Figure 8.1: Performance of EM-JED algorithm in the fading speed 0.01.

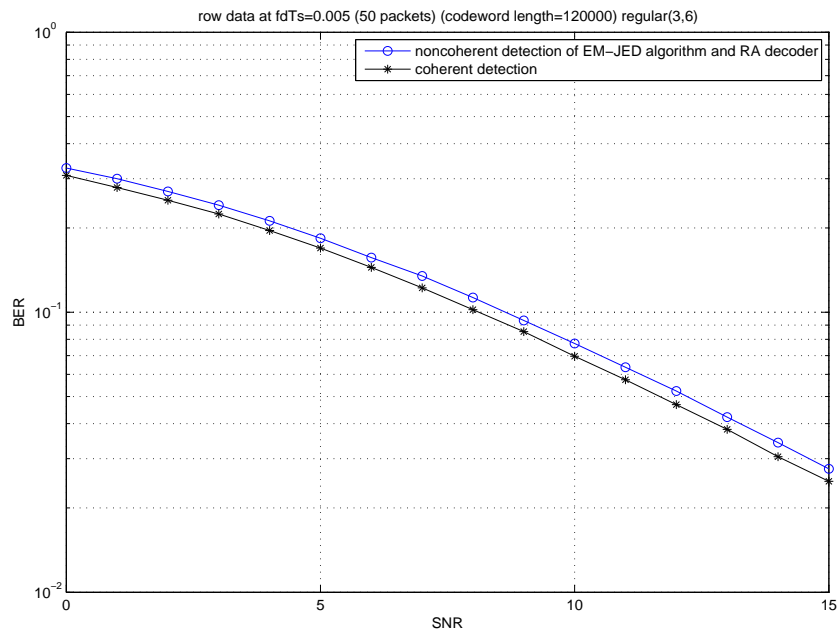


Figure 8.2: Performance of EM-JED algorithm in the fading speed 0.005.

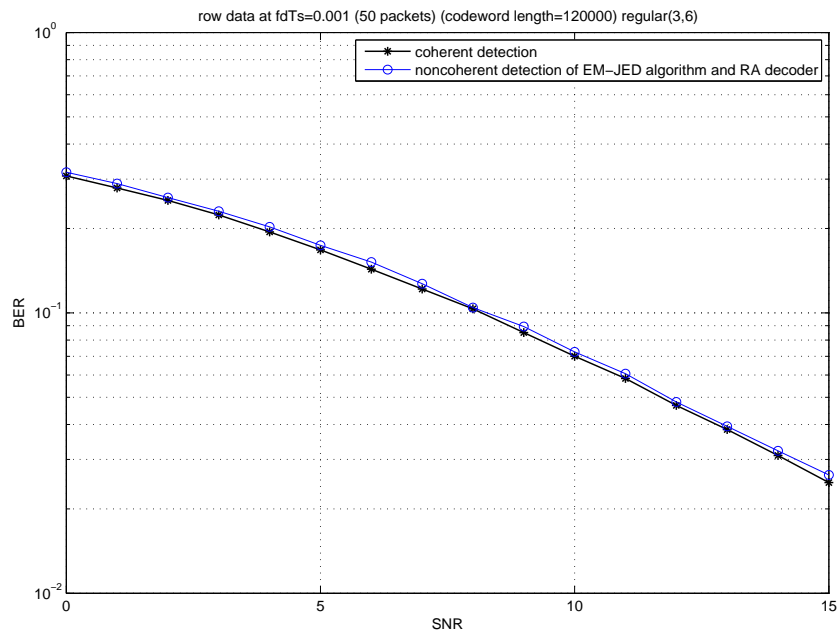


Figure 8.3: Performance of EM-JED algorithm in the fading speed 0.001.

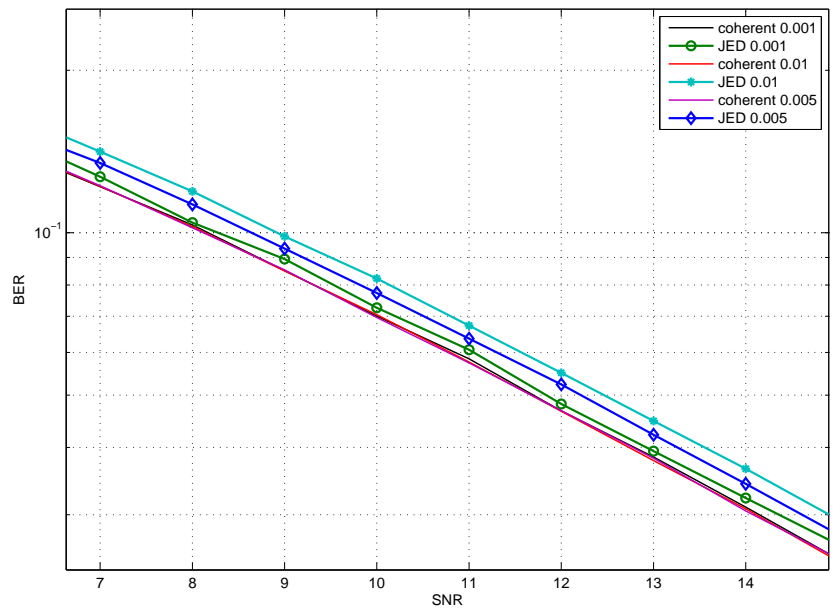


Figure 8.4: Performance of EM-JED algorithm in different fading speeds.

8.2 Performance of combined EM-JED algorithm and LDPC decoding in fading channels

8.2.1 The performance of the same codeword length 12000 in different fading speeds

In Fig. 8.5, the performance of regular (3,6) LDPC codes with codeword length 12000 in different fading speeds is shown. The LDPC code were both designed by the design criteria in Chapter 4.1. The coherence interval here is given with the inverse of the fading speed. With the same codeword length 12000, there are about 120 coherence intervals in the fading speed 0.01, 60 coherence intervals in the fading speed 0.005, and 12 coherence intervals in the fading speed 0.001.

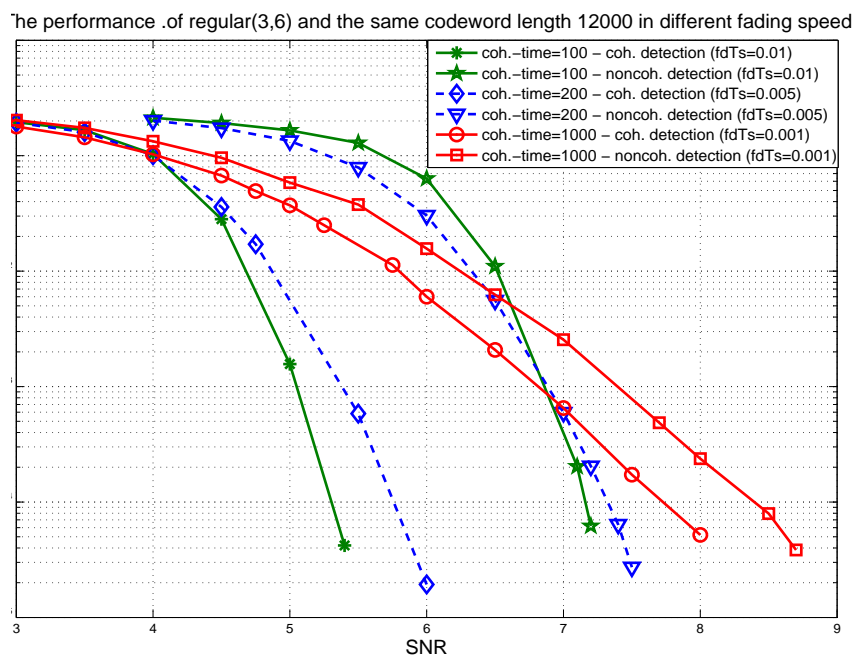


Figure 8.5: Performance of the same codeword length 12000 in different fading speeds.

In the simulation results, the slope of the performance curves with the maximum number of coherence intervals is steepest in these three fading speeds. Both in the ideal

fading channel and fading channel, the performance in the fading speed 0.01 is best and the performance in fading speed 0.001 is worst. Besides, the performance gap between the ideal fading channel and fading channel becomes smaller in the lower fading speed as mentioned above.

8.2.2 The performance of the same number of coherence intervals in different fading speeds

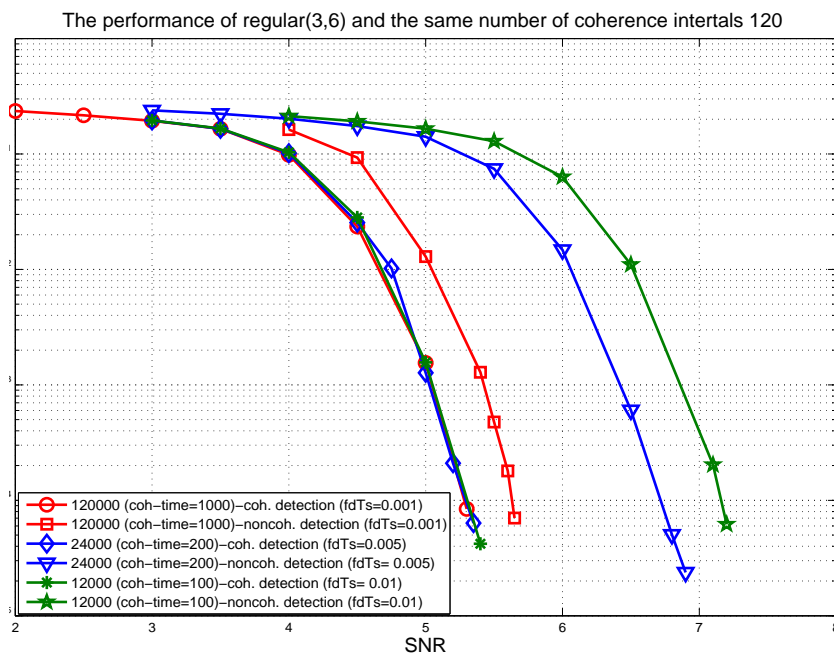


Figure 8.6: Performance of the same number of coherence intervals in different fading speeds.

In Fig. 8.6, the performance of regular (3,6) LDPC codes with 120 coherence intervals in different fading speed is shown. The codeword length becomes 24000 in the fading speed 0.005 and 120000 in the fading speed 0.001. With the same number of coherence intervals, the performance curves of ideal channel case in different fading speeds become much close. Even with the different codeword length, the performance

curves here are dominated by the number of coherence intervals.

8.2.3 The performance of the same codeword length 120000 in different fading speeds

The longest codeword length we can generate is 120000. Here we compared the performance of regular (3,6) LDPC codes with codeword length 120000 in different fading speeds. With the same codeword length 120000, there are about 1200 coherence intervals in the fading speed 0.01, 600 coherence intervals in the fading speed 0.005, and 120 coherence intervals in the fading speed 0.001.

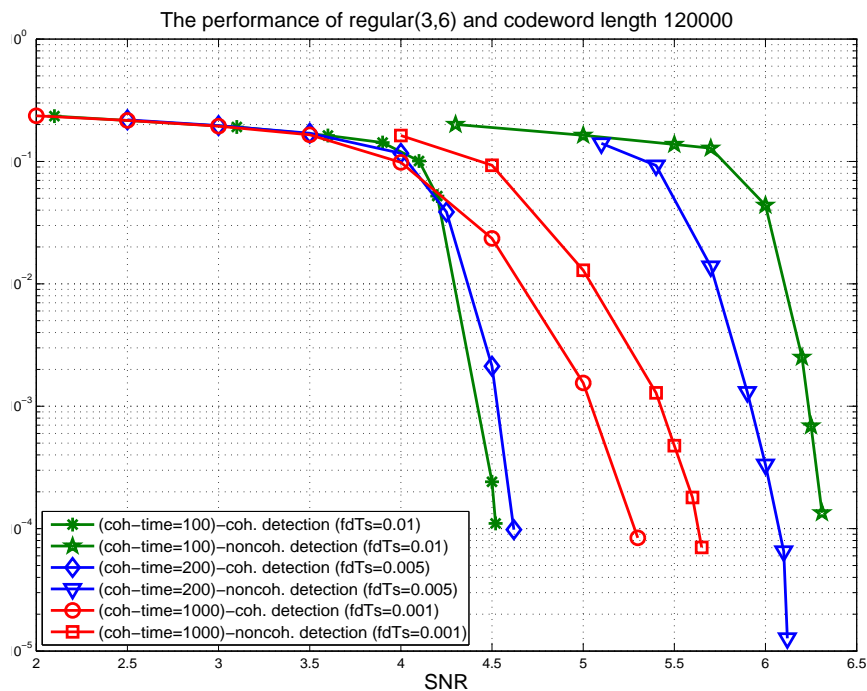


Figure 8.7: Performance of the same codeword length 120000 in different fading speeds.

The performance curves in ideal fading channels are still dominated by the number of coherence intervals. Besides, the performance gap between ideal fading channel and fading channel is still decided by the fading speed. In fading channel, the performance

in fading speed 0.001 becomes the best in these three fading speeds in Fig. 8.7.

8.3 Performance of different degree profiles with density evolution analysis

In our simulation results, we found some degree profiles which contain minimum variable degree 2 would suffer the serious error floor such as in Fig. 8.8. The degree

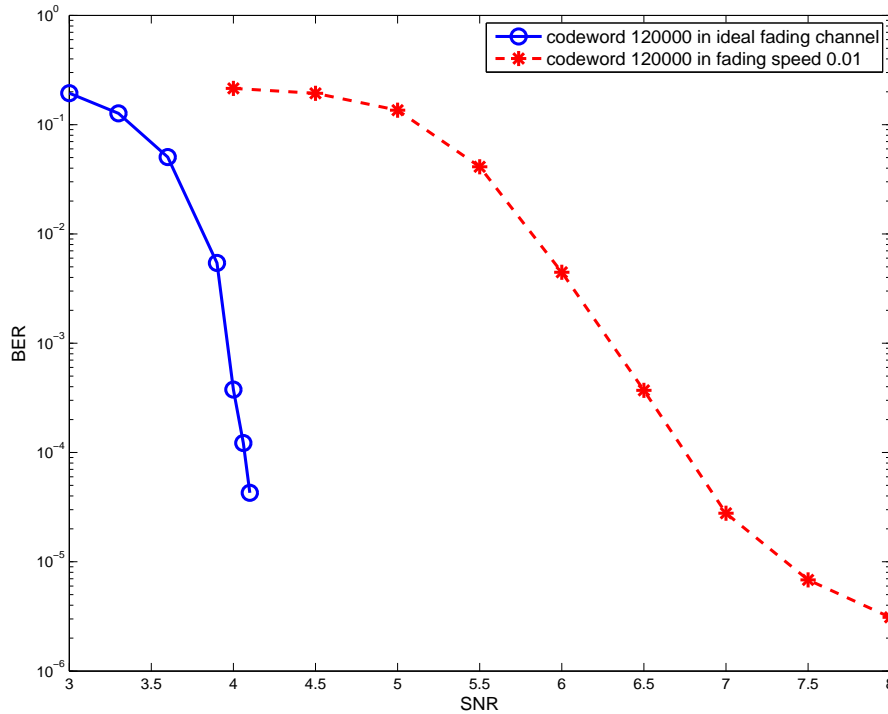


Figure 8.8: Performance of given regular-check degree profile which contains the minimum variable degree 2.

distribution pairs are shown as

$$\begin{aligned} \lambda(x) &= 0.4253x + 0.0371x^2 + 0.0159x^3 + 0.5217x^4 \\ \rho(x) &= x^5 \end{aligned} \tag{8.1}$$

However, the error floor doesn't appear in the ideal fading channel. The extrinsic message computed at the variable nodes of degree 2 might become worse with only one prior information passed from check nodes to variable nodes in fading channels.

To prevent the above situation, we only consider the degree profile in which the minimum variable degree must be larger than 3. Based on the nonlinear optimization algorithm of differential evolution, we found several check-regular degree profiles and computed its density evolution threshold in Fig. 8.9-8.14.

The density evolution threshold becomes away from the simulations with higher maximum variable degree. For example, the density evolution threshold of the degree profiles of maximum variable degree 11 is about 0.5dB away from the simulations. And the density evolution threshold of the degree profiles of maximum variable degree 19 is about 0.6dB away from the simulations. It might be caused by the mentioned problem of Gaussian approximation described in Chapter 6. The density evolution performs well in other degree profiles which contains smaller maximum variable degree.

Besides, the performance of other variable-irregular degree profiles which contain the minimum variable degree 3 are worse than the performance of regular (3,6) degree profile and so does the regular (4,8) degree profile.

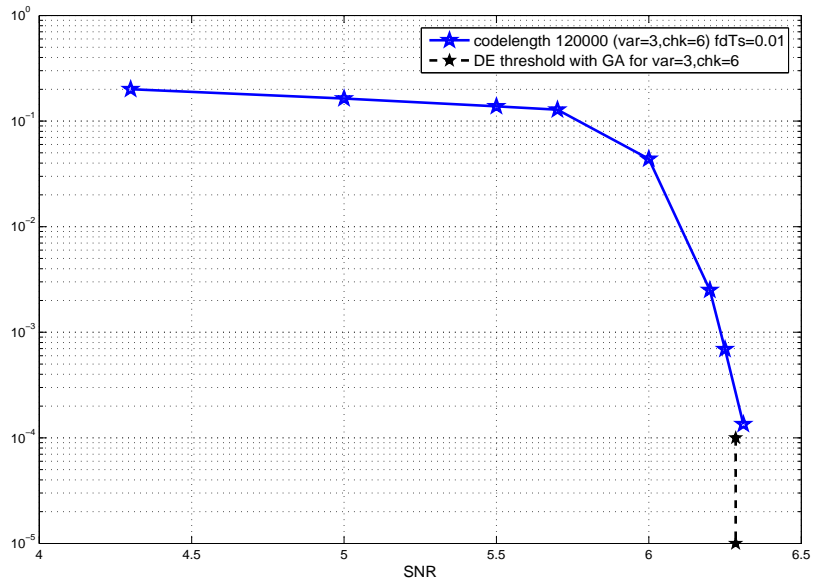


Figure 8.9: Performance of regular (3,6) LDPC code.

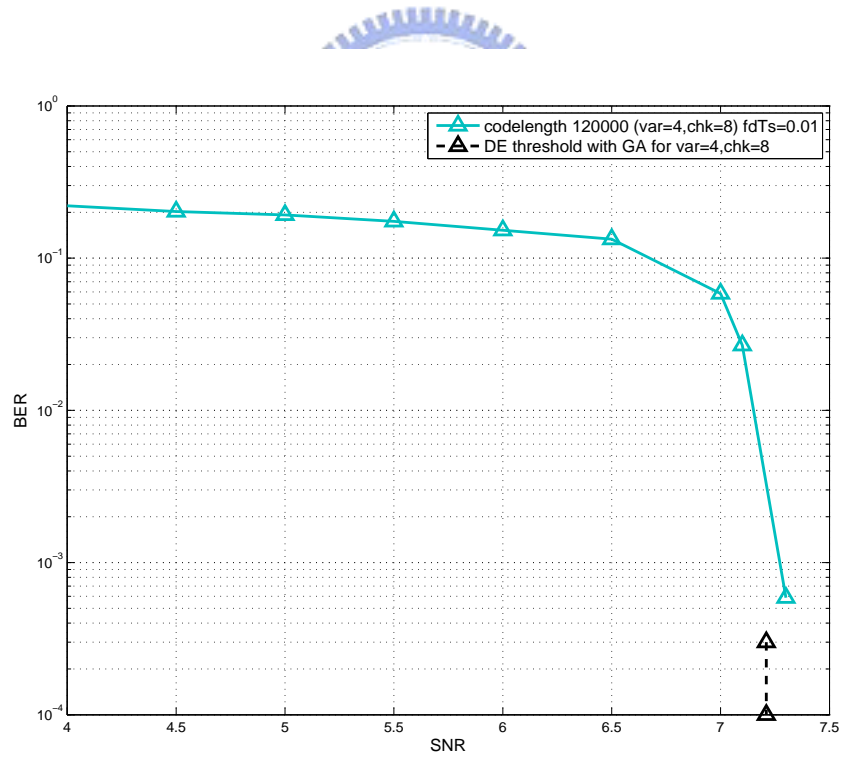


Figure 8.10: Performance of regular (4,8) LDPC code.

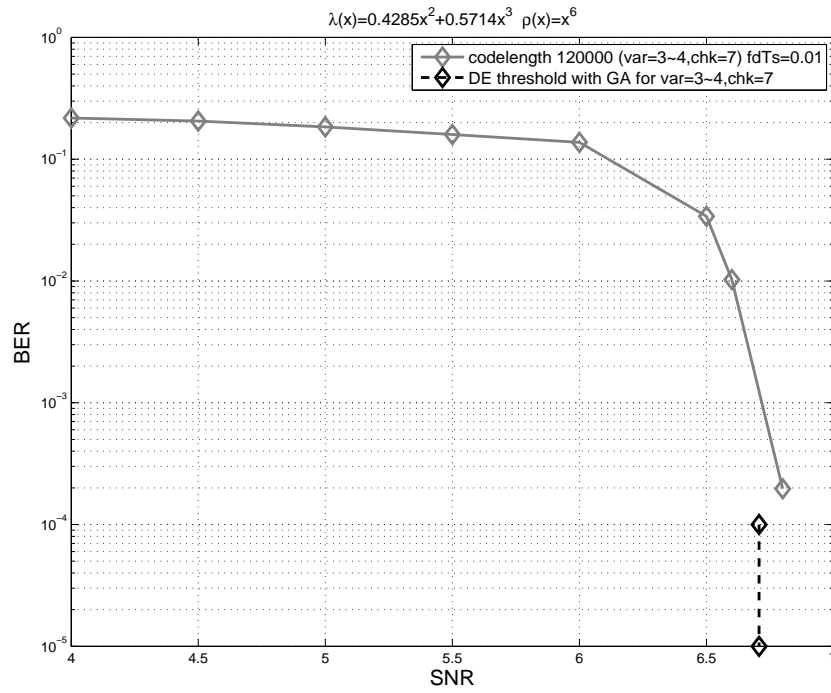


Figure 8.11: Performance of given regular-check degree profile with maximum variable degree 4.

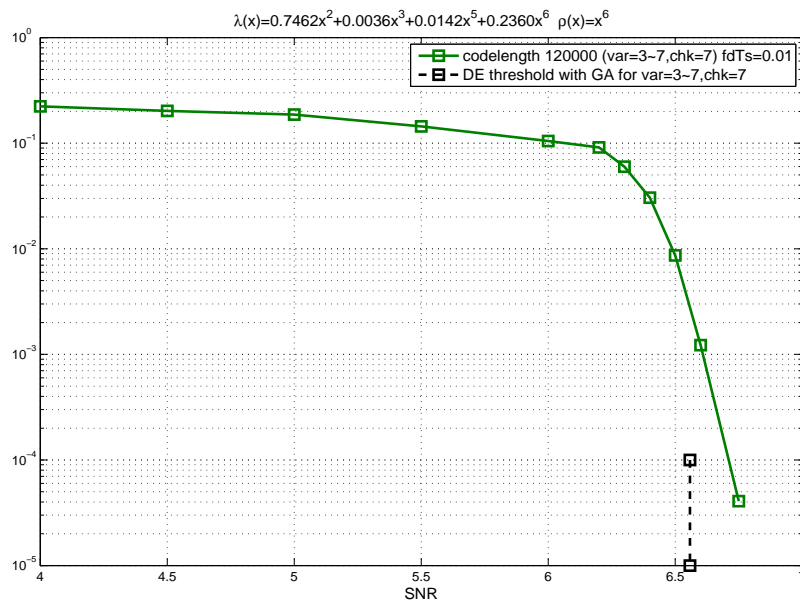


Figure 8.12: Performance of given regular-check degree profile with maximum variable degree 7.

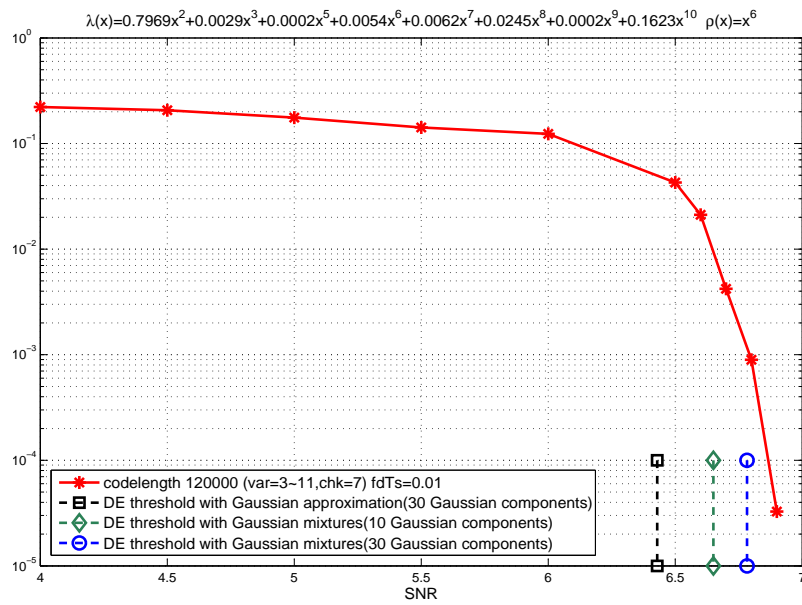


Figure 8.13: Performance of given regular-check degree profile with maximum variable degree 11.

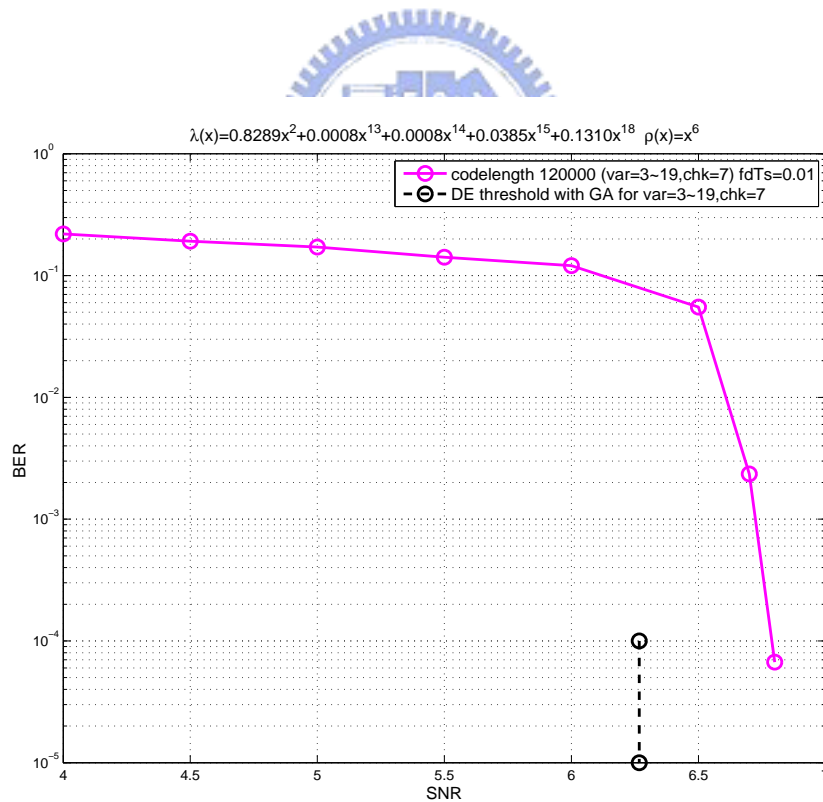


Figure 8.14: Performance of given regular-check degree profile with maximum variable degree 19.

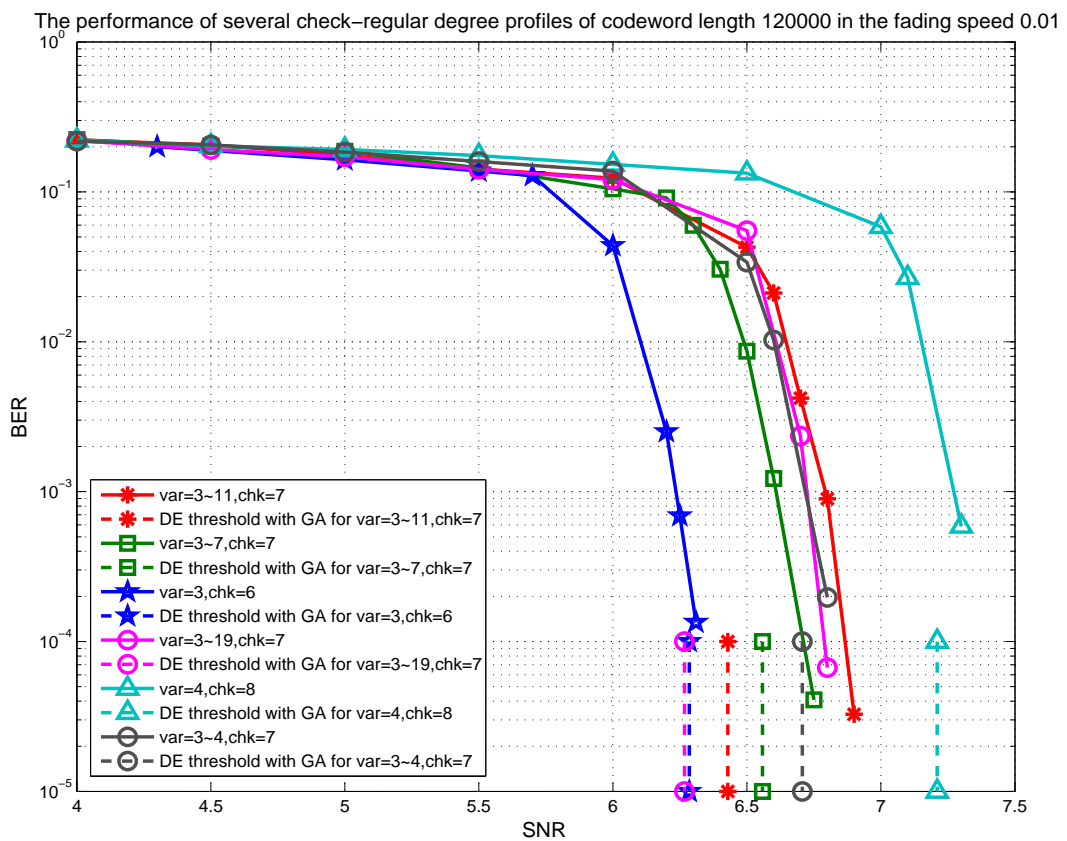


Figure 8.15: Performance of the overall generated regular-check degree profiles.

Chapter 9

Conclusions

A serially concatenated turbo transceiver of EM-JED algorithm, RA decoder and LDPC decoding is proposed in the noncoherent system. Hence without using any pilot and training symbols, the proposed serially concatenated turbo transceiver try to approach the noncoherent capacity with the LDPC code optimization. The analysis methods, such as density evolution and EXIT chart, are generally used with the symmetric Gaussian approximation. However the approximation has not been suitable for some degree profiles in the flat-fading channel. Besides, we also found that the performance of the combined EM-JED algorithm and LDPC decoding is also affected by the number of coherence intervals. Hence it might be the interesting problem to find the optimal shortest LDPC codeword length which contains the sufficient number of coherence intervals in different fading speeds. The proposed design criterion of LDPC code can be also modified for other MIMO OFDM systems.

Bibliography

- [1] S.-H. Wu, U. Mitra, and C.-C. J. Kuo, “Graph representation for joint channel estimation and symbol detection,” in *Proc. IEEE Globecom. Dallas*, Dec. 2004.
- [2] H. Zamiri-Jafarian and S. Pasupathy, “EM-based recursive estimation of channel parameters,” *IEEE Trans. on Commun.*, vol. 47, no. 9, pp. 1297 – 1302, Sep. 1999.
- [3] R. Gallager, “Low-density parity-check codes,” *IRE Trans. Inform. Theory*, pp. 21 – 28, Jan. 1962.
- [4] R. M. Tanner, “A recursive approach to low complexity codes,” *IEEE Trans. on Inform. Theory*, vol. 27, no. 5, pp. 533 – 547, Sep. 1981.
- [5] D. J. C. Mackay and R. M. Neal, “Good codes based on very sparse matrices,” in *Cryptography and Coding, 5th IMA Conf., C. Boyd, Ed., Lecture Notes in Computer Science*, 1995.
- [6] D. J. C. MacKay, “Good error-correcting codes based on very sparse matrices,” Mar. 1999, vol. 45, pp. 399 – 431.
- [7] N. Alon and M. Luby, “A linear time erasure-resilient code with nearly optimal recovery,” *IEEE Tran. on Inform. Theory*, vol. 42, no. 6, pp. 1732 – 1736, Nov. 1996.
- [8] W. E. Ryan, “An Introduction to LDPC Codes,” Aug. 2003.

- [9] V. T. Nam, P. Y. Kam, and Y. Xin, “LDPC codes with BDPSK and differential detection over flat Rayleigh fading channels,” in *Proc. of the 50th IEEE Global Telecommunications Conf. (GLOBECOM '07)*, Nov. 2007, pp. 3245 – 3249.
- [10] H. Tatsunami, K. Ishibashi, and H. Ochiai, “On the performance of LDPC codes with differential detection over Rayleigh fading channels,” in *Proc. IEEE, Vehicular Technology Conference, VTC 2006-Spring.*, May. 2006, vol. 5, pp. 2388 – 2392.
- [11] J. Zheng and B. D. Rao, “LDPC-coded MIMO systems with unknown block fading channels: soft MIMO detector design, channel estimation, and code optimization,” *IEEE Trans. on Signal Proc.*, vol. 54, no. 4, pp. 1504 – 1518, Apr. 2006.
- [12] K. Fu and A. Anastasopoulos, “Analysis and design of LDPC codes for time-selective complex-fading channels,” *IEEE Trans. on Wireless Commun.*, vol. 4, no. 3, pp. 1175 – 1185, May. 2005.
- [13] A. W. Eckford and T. E. Fuja, “LDPC codes for non-coherent block fading channels with correlation: analysis and design,” *IEEE Trans. on Commun.*, vol. 56, no. 1, pp. 70 – 80, Jan. 2008.
- [14] T. J. Richardson and R. L. Urbanke, “The capacity of low-density parity-check codes under message-passing decoding,” *IEEE Trans. on Inform. Theory*, vol. 47, no. 2, pp. 599 – 618, Feb. 2001.
- [15] S. ten Brink, “Convergence of iterative decoding,” *Electron. Lett.*, vol. 35, no. 10, pp. 806 – 808, May. 1999.
- [16] S. ten Brink, G. Kramer, and A. Ashikhmin, “Design of low-density parity-check codes for modulation and detection,” *IEEE Trans. on Comm.*, vol. 52, no. 4, pp. 670 – 678, Apr. 2004.

- [17] A. Ashikhmin, G. Kramer, and S. ten Brink, “Extrinsic information transfer functions: model and erasure channel properties,” *IEEE Trans. on Inform. Theory*, vol. 50, no. 11, pp. 2657 – 2673, Nov. 2004.
- [18] S. ten Brink, “Convergence behavior of iteratively decoded parallel concatenated codes,” *IEEE Trans. on Commun.*, vol. 49, no. 10, pp. 1727 – 1737, Oct. 2001.
- [19] S. ten Brink and G. Kramer, “Design of repeat-accumulate codes for iterative detection and decoding,” *IEEE Trans. on Signal Proc.*, vol. 51, no. 11, pp. 2764 – 2772, Nov. 2003.
- [20] S. Y. Chung, G. D. Forney, T. J. Richardson, and R. Urbanke, “On the design of low-density parity-check codes within 0.0045 dB of the Shannon limit,” *IEEE Commun.*, vol. 5, no. 2, pp. 58 – 60, Feb. 2001.
- [21] B. Lu, G. Yue, and X. Wang, “Performance analysis and design optimization of LDPC-coded MIMO OFDM systems,” *IEEE Trans. on Signal Proc.*, vol. 52, no. 2, pp. 348 – 361, Feb. 2004.
- [22] L. R. Bahl, J. Cocke, F. Jelinek, and J. Raviv, “Optimal decoding of linear codes for minimizing symbol error rate,” *IEEE Trans. on Inform. Theory*, vol. 20, no. 2, pp. 284 – 287, Mar. 1974.